RSC Advances

PAPER

Cite this: *RSC Adv.*, 2021, **11**, 36989

New quinoxaline compounds as DPP-4 inhibitors and hypoglycemics: design, synthesis, computational and bio-distribution studies†

Yasmin M. Syam,[a] Manal M. Anwar,*[a] Somaia S. Abd El-Karim,[a] Samia A. Elseginy,[b] Basma M. Essa[c] and Tamer M. Sakr[c]

Received 10th September 2021
Accepted 24th October 2021

DOI: 10.1039/d1ra06799k

rsc.li/rsc-advances

The current work represents the design and synthetic approaches of a new set of compounds **6–10** bearing the 1,4-dimethyl-2,3-dioxo-1,2,3,4-tetrahydroquinoxaline-6-sulfonamide scaffold. The biological evaluation revealed that most of the new compounds were promising selective dipeptidyl peptidase-IV (DPP-4) inhibitors and *in vivo* hypoglycemic agents utilizing linagliptin as a standard drug. The acute toxicity examination confirmed the safety profile of all compounds. Molecular docking studies related the significant DPP-4 suppression activity of compounds **9a**, **10a**, **10f**, **10g** to their nice fitting in the active pocket of DPP-4. In addition, the molecular dynamic study exhibited the stability of both **10a** and **10g** within the active site of DPP-4. The QSAR study showed that the difference between the predicted activities is very close to the experimental suppression effect. Moreover, both compounds **10a** and **10g** obeyed Lipinski's rule, indicating their efficient oral bioavailability. Compound **10a** was radiolabeled, forming the ^{131}I-SQ compound **10a** to study the pharmacokinetic profile of this set of compounds. The biodistribution pattern hit the target protein since the tracer accumulated mainly in the visceral organs where DPP-4 is secreted in a high-level, thus with consequent stimulation of insulin secretion, leading to the target hypoglycemic effect.

1. Introduction

Diabetes mellitus (DM) is an endocrine and metabolic disorder. It is considered one of the world's biggest health problems with several specific factors related to its pathogenesis. The International Diabetes Federation (IDF) reported that there were 425 million adults suffering from DM worldwide in 2017, with an alarming growth estimate at 700 million in 2045 and 90–95% are expected to be patients with type – 2 diabetes mellitus (T2DM).[1–4] The main causes of T2DM are either deficiency in insulin production by the pancreas or inactivation of some proteins participating in the insulin signaling pathway (insulin resistance).[5–8] Diabetes is usually involved with multiple complications, such as cardiovascular diseases,[9] retinopathy,[10] neuropathy,[11,12] dental and kidney diseases.[13,14] There are other complications of diabetes, including wound interference cure,[15] ketoacidosis, hyperosmolar coma,[16,17] as well as reduced immunity to pneumonia and influenza.[18,19] Recently, it has been reported that type 2 diabetes is one of the most important diseases that results in a significant increase of the risk for hospitalization and death in COVID-19 patients. Hypoglycemia and hyperglycemia are both considered as predictors for adverse outcomes in hospitalized patients. In patients with diabetes and SARS-CoV-2 infection, optimal glycemic control should be followed to reduce the likelihood of a serious COVID-19 course.[20–23] The main goal behind T2DM treatment is to decrease and maintain the level of the glycosylated hemoglobin at less than 7% to prevent the risk of the micro- and macrovascular complications related to the disease.[24]

Drugs currently used for T2DM treatment include biguanides, insulin sensitizers (thiazolidinediones), insulin secretagogues (sulphonylureas; meglitinides), and external insulin delivery (insulin analogs). The European Medicines Agency currently approved α-glucosidase inhibitors, glucagon-like peptide-1 (GLP-1) agonists, sodium-dependent glucose transporter 2 inhibitors, and the recent class of dipeptidyl peptidase-4 (DPP-4) inhibitors.[25]

DPP-4 is a multifunctional serine peptidase that cleaves N-terminal dipeptides from substrates containing Pro or Ala at the penultimate position. It is expressed in many tissues, such as the kidney, gastrointestinal tract, biliary tract, liver, placenta, uterus, prostate, skin and lymphocytes.[26] DPP4 is mainly released by fully differentiated adipocytes, and its serum levels significantly correlate with the adipocyte size. Therefore, it

[a]*Department of Therapeutic Chemistry, National Research Center, Dokki, Cairo 12622, Egypt. E-mail: manal.hasan52@live.com*
[b]*Green Chemistry Department, National Research Center, Dokki, Cairo 12622, Egypt*
[c]*Radioactive Isotopes and Generator Department, Hot Laboratories Centre, Egyptian Atomic Energy Authority (EAEA), P.O. Box 13759, Cairo, Egypt*

† Electronic supplementary information (ESI) available. See DOI: 10.1039/d1ra06799k

seems to be a marker of visceral obesity, insulin resistance, and metabolic syndrome.[27] Food intake and an increase in blood glucose stimulate the gut release of the incretin hormones, GLP-1 and glucose-dependent insulinotropic polypeptide (GIP), which in turn stimulate insulin secretion in a glucose-dependent manner. GLP-1 and GIP increase insulin biosynthesis, promote beta cell proliferation and reduce beta cell apoptosis. DPP-4 rapidly inactivates both GLP-1 and GIP. Therefore, inhibition of DPP-4 leads to prolongation of the circulating half-lives of both GLP-1 and GIP.[24,28,29] It has been shown that DPP-4 inhibitors block the inactivation of the incretin hormones, resulting in the stimulation of insulin secretion, inhibition of glucagon secretion, and thereby improvement of glucose control.[3,30] Multiple DPP-4 suppressors are currently approved by the United States Food and Drug Administration. Sitagliptin was the first DPP-4 inhibitor, approved by FDA,[31] followed by Vildagliptin,[32] Saxagliptin,[33] Alogliptin,[34] and Linagliptin.[35] New candidates continued to be granted approval: Anagliptin,[36] Gemigliptin,[37] Teneligliptin[38] in 2012, Evogliptin,[39] Omarigliptin[40] and Trelagliptin[41] in 2015, and Gosogliptin[42] in 2016 (Fig. 1).

Despite the efficiency, safety and low risk for hypoglycemia and weight gain of the class of DPP-4 inhibitors,[43] some safety apprehension was reported due to the clinical use. Increased

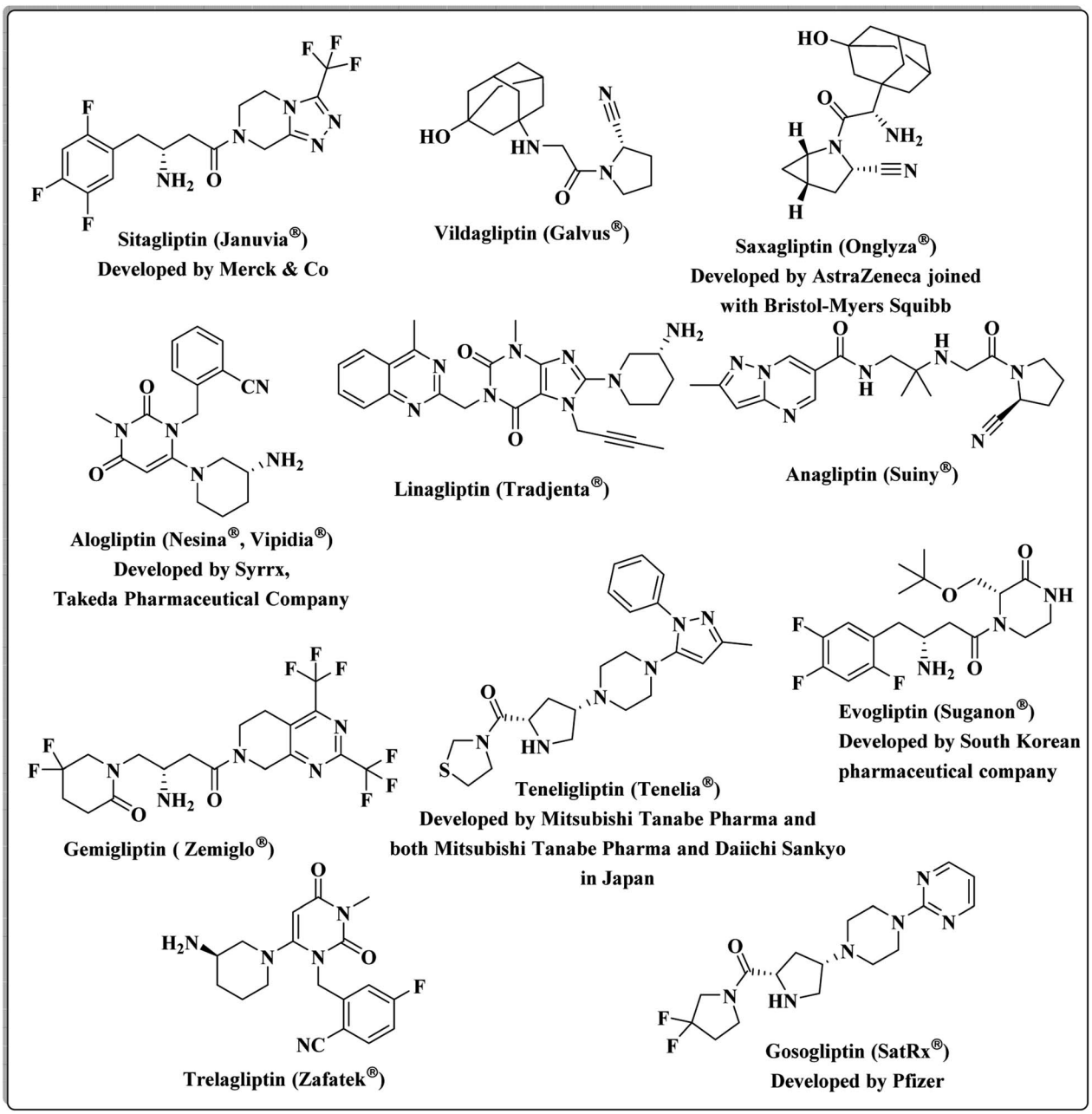

Fig. 1 The current approved DPP-4 inhibitors.

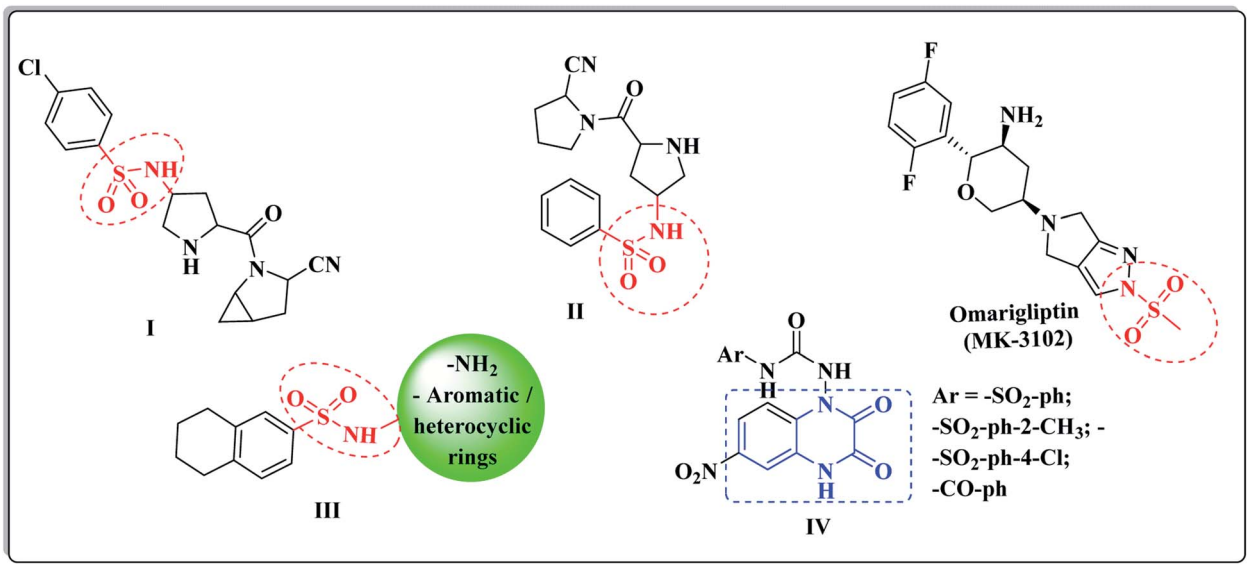

Fig. 2 Different DPP-4 inhibitors bearing sulfonamide and quinoxaline cores.

risk of heart failure, severe and acute pain of joints, pancreatitis and pancreatic cancer were reported.[43,44] Accordingly, it is essential to discover new and safer DPP-4 inhibitors that will ultimately encourage their uses in clinics.

Based on its wide spectrum of biological activities, the sulphonamide moiety ($-SO_2NH_2$) is an efficacious pharmacophore in the medicinal chemistry and drug discovery field.[45,46] The sulfonyl functionality is not only able to bind with the amino acid residues of the active pocket of the biological targets with hydrogen bonds, but it also incorporates with the structural core ring and constrains the side chains, allowing their special conformations that perfectly fit in the active pockets.[47] Different laboratory research studies have reported that the sulfonamide compounds **I** and **II** represented the potent DPP-IV inhibitory activity of the IC_{50} values, 6.7 and 39 nM, respectively.[48] (Fig. 2). Furthermore, Omarigliptin (MK-3102) is a sulfonamide-based DPP-4 inhibitor that is currently under development by Merck & Co. It is a long-acting, oral and once-weekly dosing

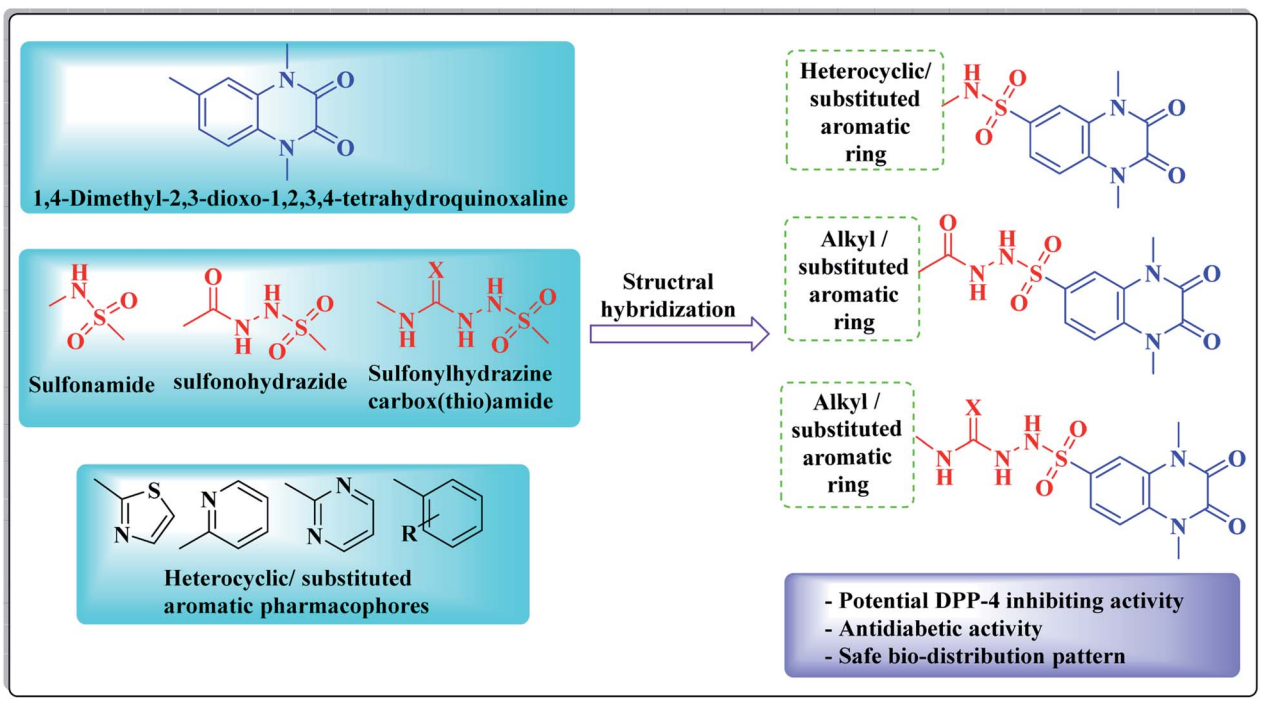

Fig. 3 The design strategy of the new quinoxaline-sulfonamide compounds.

antidiabetic drug, which makes it unique among the other members of this class.[49] In addition, our previous efforts to develop a new series of tetralin-sulphonamide derivatives introduced potent candidates of selective DPP-4 suppression activity **III** with IC_{50} values in the nanomolar range[50] (Fig. 2).

The quinoxaline nucleus constitutes a rising biomedical class of low-molecular weight heterocyclic compounds producing potential antidiabetic activity.[51–53] A chemical library of nearly 32 000 compounds (Korea Chemical Bank) was screened as DPP-4 inhibitors using high throughput screening (HTS) techniques, which resulted in discovering various quinoxalinedione derivatives as potent DPP-IV inhibitors **IV** (ref. 54) (Fig. 2). In addition, the quinoxaline scaffold is bioisosteric to the quinazoline ring, which is a major fragment of the Linagliptin structure, and it constituted the major core of different antidiabetic agents of potent DPP-4 inhibition activity.[55,56]

In view of the synergistic activity that is usually accomplished by molecular hybridization of different bioactive pharmacophores, this work represents the design and synthesis of new derivatives bearing a 1,4-dimethyl-2,3-dioxo-1,2,3,4-tetrahydroquinoxaline ring system that is conjugated at position-6 with different alkyl, heterocyclic or substituted aromatic rings *via* either sulfonamide, sulfonohydrazide and/or sulfonyl hydrazine-carboxy(thio)amide linkers aiming to gain new candidates having potential DPP-4 inhibitory activity, resulting in potent antidiabetic effect (Fig. 3). The new compounds were evaluated as DPP-4 suppressors, as well as hypoglycemic agents. As representative examples, the inhibitory activity of two promising compounds was assessed against DPP-8/9 to examine the selectivity of the newly synthesized compounds over other DPP family members, such as DPP-8 and DPP-9. A docking study has been performed for the promising active derivatives to find out the key structural parameters that are vital for the binding modes with the active site of DPP-4 in comparison to linagliptin as a reference drug. In addition, the quantitative structure activity relationship (QSAR) of the active set of new derivatives was performed to detect the descriptors, which might be correlated to the hypoglycemic activity. Furthermore, obeying Lipinski's rule criteria was assessed for the new analogues to find out their oral bioavailability efficiency. Additionally, a biodistribution study was carried out for one of the promising hypoglycemic candidates as a representative example to investigate its *in vivo* pharmacokinetic behavior and body organ uptakes, besides its elimination pathway *via* its ^{131}I compound complex radiolabeling.

2. Experimental

2.1. Chemistry

All melting points are uncorrected and were taken in open capillary tubes using the electrothermal apparatus 9100. Elemental microanalyses were carried out at the Microanalytical Unit, Central Services Laboratory, National Research Centre, Dokki, Cairo, Egypt, using a VarioElementar, and were found within ±0.5% of the theoretical values. Infrared spectra were recorded on a Jasco FT/IR-6100, Fourier transform infrared spectrometer at the cm^{-1} scale using the KBr disc technique at the Central Services Laboratory, National Research Centre, Dokki, Cairo, Egypt. ^1H NMR and ^{13}C NMR spectra were obtained by using a JEOL AS-500 NMR spectrometer (with operating frequencies of 500 MHz for ^1H using TMS as an internal standard and 125 MHz for ^{13}C) at the Central Services Laboratory, National Research Centre, Dokki, Cairo, Egypt. Chemical shifts (δ) are reported in parts per million (ppm) and coupling constants (J) are reported in Hertz (Hz). The mass spectra were measured with a GC MS-Qp1000EX Shimadzu, Cairo University, Cairo, Egypt. The follow up of the reactions and checking the purity of the compounds were made by TLC on silica gel-precoated aluminium sheets (Type 60, F 254, Merck, Darmstadt, Germany) using chloroform/petroleum ether 40–60 (5 : 1, v/v), and the spots were detected by exposure to UV lamp at λ_{254} nanometer for a few seconds and by iodine vapor. The chemical names given for the prepared compounds are according to the IUPAC system. The starting and the intermediate compounds; quinoxaline-2,3(1*H*,4*H*)-dione (**1**) 1,4-dimethylquinoxaline-2,3(1*H*,4*H*)-dione (**2**) and 1,4-dimethyl-2,3-dioxo-1,2,3,4-tetrahydroquinoxaline-6-sulfonyl chloride (**3**) 1,4-dimethyl-1,4-dihydroquinoxaline-2,3-dione (**4**) and 1,4-dimethyl-2,3-dioxo-1,2,3,4-tetrahydroquinoxaline-6-sulfonyl chloride (**5**) were prepared according to the reported methods.[57,58]

2.1.1. General method for the preparation of 1,4-dimethyl-2,3-dioxo-N-(heterocyclic/substituted aromatic)-1,2,3,4-tetrahydro quinoxaline-6-sulfonamide 6a–f. A mixture of dimethyl-2,3-dioxo-1,2,3,4-tetrahydroquinoxaline-6-sulfonyl chloride (**3**) (2.88 g, 10 mmol) and the appropriate primary amines, namely, 2-aminothiazole, 4-acetylaniline, 4-aminobenzoic acid, 4-fluoroaniline, 4-bromoaniline and/or 2-aminothiophenol (10 mmol) in absolute ethanol (10 mL), was refluxed for 3 h. The formed precipitate was filtered, washed several times with pet. ether, dried and crystallized from ethanol to afford the titled compounds **6a–f**, respectively.

*2.1.1.1. 1,4-Dimethyl-2,3-dioxo-N-(thiazol-2-yl)-1,2,3,4-tetrahydroquinoxaline-6-sulfonamide (**6a**).* Yield (73%), m.p. 207–209 °C, IR (ν_{max}/cm^{-1}): 3344 (NH), 3062 (CH, aromatic), 2999 (CH-alicyclic), 1685 (2C=O), 1381, 1180 (SO_2), ^1H NMR (DMSO-d_6, δ ppm): 3.48 (s, 6H, $2CH_3$), 6.58 (s, 1H, NH, exchangeable with D_2O), 6.75, 7.08 (2d, 2H, aromatic-H, J = 6.21 Hz), 7.24–7.52 (m, 3H, aromatic-H), ^{13}C NMR (DMSO-d_6, δ ppm): 30.35 ($2CH_3$), 114.57, 116.29, 122.47, 123.28, 128.24, 133.56, 139.06 (Ar–C), 158.48 (2C=O), 168.38 (C–S, thiazole), MS, *m*/*z* (%): 353 [M^+ + 1] (20.84), 352 [M^+] (16.38), analysis for $C_{13}H_{12}N_4O_4S_2$ (352.38): calcd % C, 44.31; H, 3.43; N, 15.90; S, 18.20, found: % C, 44.53; H, 3.65; N, 16.08; S, 18.36.

*2.1.1.2. N-(4-Acetylphenyl)-1,4-dimethyl-2,3-dioxo-1,2,3,4-tetrahydroquinoxaline-6-sulfonamide (**6b**).* Yield (75%), m.p. 121–123 °C, IR (ν_{max}/cm^{-1}): 3309 (NH), 3097 (CH, aromatic), 2978 (CH-alicyclic), 1685, 1670 (3C=O), 1384, 1145 (SO_2), ^1H NMR (DMSO-d_6, δ ppm): 3.08 (s, 3H, $-COCH_3$), 3.55 (s, 6H, $2CH_3$), 6.58, 6.83 (2d, 4H, aromatic-H, J = 5.15 Hz), 7.55–7.65 (m, 4H, 3-aromatic-H + NH, exchangeable with D_2O), ^{13}C NMR (DMSO-d_6, δ ppm): 25.68, 30.35 ($3CH_3$), 116.35, 116.69, 122.09, 123.86, 130.27, 133.56, 139.06, 140.25, 140.46, 144.39 (Ar–C), 158.48, 170.06 (3C=O), MS, *m*/*z* (%): 387 [M^+] (25.98), analysis for

$C_{18}H_{17}N_3O_5S$ (387.41), calcd% C, 55.80; H, 4.42; N, 10.85; S, 8.28. Found: % C, 55.86; H, 4.63; N, 11.07; S, 8.42.

*2.1.1.3. 4-(1,4-Dimethyl-2,3-dioxo-1,2,3,4-tetrahydroquinoxaline-6-sulfonamido)benzoic acid (**6c**).* Yield (72%), m.p. 242–244 °C, IR (ν_{max}/cm^{-1}): 3341 (OH), 3197 (NH), 3062 (CH, aromatic), 2954 (CH-alicyclic), 1710, 1670 (3C=O), 1350, 1161 (SO_2). ^{1}H NMR (DMSO-d_6, δ ppm): 3.48 (s, 6H, 2CH_3), 6.68 (s, 1H, NH, exchangeable with D_2O), 7.23, 7.35 (2d, 4H, aromatic-H, J = 9.00 Hz), 7.67–7.81 (m, 3H, aromatic-H), 10.08 (s, 1H, OH, exchangeable with D_2O), ^{13}C NMR (DMSO-d_6, δ ppm): 30.33 (2CH_3), 115.37, 116.38, 120.27, 122.89, 126.42, 128.43, 133.56, 135.38, 139.06, 140.25 (Ar–C), 156.74, 168.39 (3C=O), MS, m/z (%): 390 [M$^+$ + 1] (38.07), 389 [M$^+$] (36.91), analysis for $C_{17}H_{15}N_3O_6S$ (389.38), calcd% C, 52.44; H, 3.88; N, 10.79; S, 8.23, found: % C, 52.69; H, 4.07; N, 10.62; S, 8.44.

*2.1.1.4. N-(4-Fluorophenyl)-1,4-dimethyl-2,3-dioxo-1,2,3,4-tetrahydroquinoxaline-6-sulfonamide (**6d**).* Yield (74%), m.p. 216–218 °C, IR (ν_{max}/cm^{-1}): 3174 (NH), 3062 (CH, aromatic), 2951 (CH-alicyclic), 1685 (2C=O), 1334, 1157 (SO_2). ^{1}H NMR (DMSO-d_6, δ ppm): 3.50 (s, 6H, 2CH_3), 6.64 (s, 1H, NH, exchangeable with D_2O), 7.08, 7.11 (2d, 4H, aromatic-H, J = 6.00 Hz), 7.53–7.62 (m, 3H, aromatic-H), ^{13}C NMR (DMSO-d6, δ ppm): 30.37 (2CH_3), 113.44, 116.09, 116.31, 116.53, 122.40, 123.32, 123.40, 128.24, 131.34, 134.24, 154.03, 154.27, 158.42 (Ar–C), 160.82 (2C=O), MS, m/z (%): 363 [M$^+$] (30.42), analysis for $C_{16}H_{14}FN_3O_4S$ (363.36), calcd% C, 52.89; H, 3.88; N, 11.56; S, 8.82, found: % C, 53.05; H, 3.90; N, 11.73; S, 9.04.

*2.1.1.5. N-(4-Bromophenyl)-1,4-dimethyl-2,3-dioxo-1,2,3,4-tetrahydroquinoxaline-6-sulfonamide (**6e**).* Yield (72%), m.p. 100–102 °C, IR (ν_{max}/cm^{-1}): 3279 (NH), 3062 (CH, aromatic), 2958 (CH-alicyclic), 1685 (2C=O), 1357, 1154 (SO_2), ^{1}H NMR (DMSO-d_6, δ ppm): 3.48 (s, 6H, 2CH_3), 6.70 (s, 1H, NH, exchangeable with D_2O), 7.12, 7.20 (2d, 4H, aromatic-H, J = 6.00 Hz), 7.53–7.62 (m, 3H, aromatic-H). ^{13}C NMR (DMSO-d_6, δ ppm): 30.28 (2CH_3), 116.29, 117.37, 117.72, 122.09, 123.38, 127.53, 131.59, 133.46, 137.59, 149.80 (Ar–C), 156.62 (2C=O), MS, m/z (%): 426 [M + 2]$^+$ (18.67), 424 [M$^+$] (38.94), analysis for $C_{16}H_{14}BrN_3O_4S$ (424.27), calcd% C, 45.30; H, 3.33; N, 9.90; S, 7.56, found: % C, 45.37; H, 3.78; N, 10.07; S, 7.72.

*2.1.1.6. N-(2-Mercaptophenyl)-1,4-dimethyl-2,3-dioxo-1,2,3,4-tetrahydroquinoxaline-6-sulfonamide (**6f**).* Yield (74%), m.p. 78–80 °C, IR (ν_{max}/cm^{-1}): 3299 (NH), 3062 (CH, aromatic), 2954 (CH-alicyclic), 1678 (2C=O), 1384, 1157 (SO_2). ^{1}H NMR (DMSO-d_6, δ ppm): 3.43 (s, 6H, 2CH_3), 5.41 (s, 1H, SH, exchangeable with D_2O), 6.71 (s, 1H, NH, exchangeable with D_2O), 6.90–7.11 (m, 7H, aromatic-H), ^{13}C NMR (DMSO-d$_6$, δ ppm): 30.37 (2CH_3), 115.26, 116.53, 116.94, 119.65, 122.40, 123.45, 123.86, 128.24, 131.59, 132.24, 135.87, 150.20 (Ar–C), 158.57 (2C=O), MS, m/z (%): 377 [M$^+$] (40.02), analysis for $C_{16}H_{15}N_3O_4S_2$ (377.44), calcd% C, 50.91; H, 4.01; N, 11.13; S, 16.99, found: % C, 51.07; H, 3.89; N, 11.36; S, 17.09.

2.1.2. General method for the preparation of 1,4-dimethyl-2,3-dioxo-N-(4-substituted sulfamoylphenyl)-1,2,3,4-tetra hydroquinoxaline-6-sulfonamide 7a–d. To a solution of the sulfonyl chloride derivative **5** (10 mmol, 2.88 g) in absolute ethanol (30 mL), different sulfa drugs (10 mmol), namely, sulfanilamide, sulfathiazole, sulfapyridine and/or sulfapyrimidine, were added in the presence of a catalytic amount of triethylamine. The reaction mixture was refluxed for 6 h. The formed precipitate was collected by filtration and crystallized from isopropanol to give the derivatives **7a–d**, respectively.

*2.1.2.1. 1,4-Dimethyl-2,3-dioxo-N-(4-sulfamoylphenyl)-1,2,3,4-tetrahydroquinoxaline-6-sulfonamide (**7a**).* Yield (81%), m.p. 162–164 °C, IR (ν_{max}/cm^{-1}): 3383, 3317 (NH_2, forked), 3244 (NH), 3070 (CH, aromatic), 2954 (CH-alicyclic), 1670 (2C=O), 1384, 1149 (SO_2), ^{1}H NMR (DMSO-d_6, δ ppm): 3.48 (s, 6H, 2CH_3), 4.85 (s, 2H, NH_2, exchangeable with D_2O), 6.20 (s, 1H, NH, exchangeable with D_2O), 7.02, 7.16 (2d, 4H, aromatic-H, J = 8.01 Hz), 7.47–7.60 (m, 3H, aromatic-H), ^{13}C NMR (DMSO-d_6, δ ppm): 30.36 (2CH_3), 115.03, 116.28, 121.26, 124.37, 127.79, 132.71, 134.29, 140.05, 141.47, 143.82 (Ar–C), 155.65 (2C=O), MS, m/z (%): 424 [M$^+$] (34.82), analysis for $C_{16}H_{16}N_4O_6S_2$ (424.45), calcd% C, 45.28; H, 3.80; N, 13.20; S, 15.11, found: % C, 45.39; H, 3.73; N, 13.46; S, 15.34.

*2.1.2.2. 1,4-Dimethyl-2,3-dioxo-N-(4-(N-thiazol-2-ylsulfamoyl) phenyl)-1,2,3,4-tetrahydro quinoxaline-6-sulfonamide (**7b**).* Yield (83%), m.p. >300 °C, IR (ν_{max}/cm^{-1}): 3217 (2NH), 3066 (CH, aromatic), 2954 (CH-alicyclic), 1685 (2C=O), 1388, 1134 (SO_2), ^{1}H NMR (DMSO-d_6, δ ppm): 3.48 (s, 6H, 2CH_3), 5.92 (s, 1H, NH, exchangeable with D_2O), 6.61, 7.02 (2d, 4H, aromatic-H, J = 8.01 Hz), 7.35–7.58 (m, 4H, aromatic-H, NH), 7.84, 8.03 (2d, 2H, aromatic-H, J = 8.01 Hz), ^{13}C NMR (DMSO-d_6, δ ppm): 30.42 (2CH_3), 112.21, 116.36, 122.05, 123.62, 131.89, 134.56, 135.28, 137.41, 137.72, 138.09, 140.05 (Ar–C), 155.65 (2C=O), 165.68 (C–S, thiazole), MS, m/z (%): 507 [M$^{\cdot+}$] (36.82), analysis for $C_{19}H_{17}N_5O_6S_3$ (507.55), calcd % C, 44.96; H, 3.38; N, 13.80; S, 18.95. Found: % C, 45.07; H, 3.47; N, 13.69; S, 19.06.

*2.1.2.3. 1,4-Dimethyl-2,3-dioxo-N-(4-(N-pyridin-2-ylsulfamoyl) phenyl)-1,2,3,4-tetrahydro quinoxaline-6-sulfonamide (**7c**).* Yield (85%), m.p. 100–102 °C, IR (ν_{max}/cm^{-1}): 3232, 3145 (2NH), 3093 (CH, aromatic), 2954 (CH-alicyclic), 1678 (2C=O), 1388, 1134 (SO_2), ^{1}H NMR (DMSO-d_6, δ ppm): 3.44 (s, 6H, 2CH_3), 5.92 (s, 1H, NH, exchangeable with D_2O), 6.50, 7.02 (2d, 4H, aromatic-H, J = 8.01 Hz), 7.47–7.60 (m, 4H, aromatic-H, NH), 7.66, 7.97 (2d, 4H, aromatic-H, J = 8.01 Hz), ^{13}C NMR (DMSO-d_6, δ ppm): 30.38 (2CH_3), 110.27, 113.16, 115.11, 120.37, 122.35, 125.82, 126.26, 132.57, 135.34, 140.49, 153.57, 154.17 (Ar–C), 158.87 (2C=O), MS, m/z (%): 501 [M$^+$] (33.27), analysis for $C_{21}H_{19}N_5O_6S_2$ (501.53), calcd % C, 50.29; H, 3.82; N, 13.96; S, 12.79, found: % C, 50.42; H, 3.99; N, 14.06; S, 12.89.

*2.1.2.4. 1,4-Dimethyl-2,3-dioxo-N-(4-(N-pyrimidin-2-yl) sulfamoyl)phenyl-1,2,3,4-tetrahydro quinoxaline-6-sulfonamide (**7d**).* Yield (83%), m.p. 235–237 °C, IR (ν_{max}/cm^{-1}): 3240, 3232 (2NH), 3055 (CH, aromatic), 2978 (CH-alicyclic), 1680 (2C=O), 1380, 1158 (SO_2), ^{1}H NMR (DMSO-d_6, δ ppm): 3.49 (s, 6H, 2CH_3), 5.99 (s, 1H, NH, exchangeable with D_2O), 6.51 (d, 2H, aromatic-H, J = 8.01 Hz), 6.96–6.98 (m, 4H, aromatic-H), 7.56, 8.43 (2d, 4H, aromatic-H, J = 8.01 Hz), 8.90 (s, 1H, NH, exchangeable with D_2O), ^{13}C NMR (DMSO-d$_6$, δ ppm): 30.45 (2CH_3), 112.29, 112.56, 115.11, 120.10, 121.59, 126.94, 127.79, 130.74, 134.29, 139.79, 141.60, 144.36, 154.28, 154.34 (Ar–C), 158.87 (2C=O). MS, m/z (%): 502 [M$^+$] (37.36), analysis for $C_{20}H_{18}N_6O_6S_2$ (502.52), calcd

% C, 47.80; H, 3.61; N, 16.72; S, 12.76, found: % C, 47.74; H, 3.74; N, 16.86; S, 12.93.

2.1.3. General method for the preparation of 1,4-dimethyl-2,3-dioxo-1,2,3,4-tetrahydro quinoxaline-6-sulfonohydrazide (8). To a solution of the sulfonyl chloride derivative **5** (10 mmol, 2.80 g) in ethanol (30 mL), hydrazine hydrate 98% (40 mmol, 2 mL) was added. The reaction mixture was stirred at room temperature for 7 h. The formed precipitate was collected by filtration and crystallized from ethanol to give the desired product **8** as a white powder.

Yield (80%), m.p. 184–186 °C, IR (ν_{max}/cm^{-1}): 3396, 3320 (NH_2), 3193 (NH), 3057 (CH, aromatic), 2953 (CH-aliphatic), 1692 (2C=O), 1327, 1166 (SO_2), ^{1}H NMR (DMSO-d_6, δ ppm): 3.43 (s, 6H, 2CH_3), 4.57 (s, 2H, NH_2, exchangeable with D_2O), 5.92 (s, 1H, NH, exchangeable with D_2O), 7.47–7.60 (m, 3H, aromatic-H), ^{13}C NMR (DMSO-d_6, δ ppm): 30.37 (2CH_3), 120.34, 122.08, 126.47, 131.26, 135.53 (Ar–C), 158.87 (2C=O), MS, *m*/*z* (%): 285 [M + 1]$^+$ (37.03), 284 [M$^+$] (29.81), analysis for $C_{10}H_{12}N_4O_4S$ (284.29), calcd% C, 42.25; H, 4.25; N, 19.71; S, 11.28, found: % C, 42.38; H, 4.32; N, 19.83; S, 11.42.

2.1.4. General method for the preparation of N′-substituted-1,4-dimethyl-2,3-dioxo-1,2,3,4-tetrahydroquinoxaline-6-sulfonohydrazide 9a–c. A solution of the sulfonohydrazide derivative **8** (10 mmol, 2.84 g) and various acid chloride derivatives, namely, acetyl chloride, 2-chloroacetyl chloride and benzoyl chloride (10 mmol) in pyridine (20 mL), was refluxed for 6 h. After completion of the reaction, the solution was poured onto ice/H_2O and neutralized with HCl. The formed precipitate was collected by filtration, washed several times with water, and crystallized from isopropanol to give the corresponding derivatives **9a–c**.

*2.1.4.1. N′-Acetyl-1,4-dimethyl-2,3-dioxo-1,2,3,4-tetrahydroquinoxaline-6-sulfonohydrazide (**9a**).* Yield (65%), m.p. 136–138 °C, IR (ν_{max}/cm^{-1}): 3433–3234 (2NH), 3006 (CH, aromatic), 2931 (CH-alicyclic), 1671, 1660 (3C=O), 1291, 1178 (SO_2), ^{1}H NMR (DMSO-d_6, δ ppm): 2.05 (s, 3H, $COCH_3$), 3.48 (s, 6H, 2CH_3), 7.46, 7.68 (2d, 2H, aromatic-H, J = 10.21 Hz), 8.04 (s, 1H, aromatic-H), 9.16, 10.03 (2s, 2H, 2NH, exchangeable with D_2O), ^{13}C NMR (DMSO-d$_6$, δ ppm): 20.50, 30.38 (3CH_3), 122.37, 125.48, 128.57, 131.20, 135.85, 137.08 (Ar–C), 155.31, 158.27, 168.30 (3C=O), MS, *m*/*z* (%): 326 [M$^+$] (36.26), analysis for $C_{12}H_{14}N_4O_5S$ (326.33), calcd % C, 44.17; H, 4.32; N, 17.17; S, 9.83, found: % C, 44.38; H, 3.95; N, 17.26; S, 10.20.

*2.1.4.2. N′-(2-Chloroacetyl)-1,4-dimethyl-2,3-dioxo-1,2,3,4-tetrahydroquinoxaline-6-sulfono hydrazide (**9b**).* Yield (70%), m.p. 136–138 °C, IR (ν_{max}/cm^{-1}): 3433, 3234 (2NH), 3006 (CH, aromatic), 2931 (CH-alicyclic), 1671, 1665 (3C=O), 1291, 1178 (SO_2), ^{1}H NMR (DMSO-d_6, δ ppm): 3.50 (s, 6H, 2CH_3), 4.21 (s, 2H, CH_2), 7.41–7.47 (m, 2H, aromatic-H), 7.55 (s, 1H, aromatic-H), 9.16, 10.03 (2s, 2H, 2NH, exchangeable with D_2O), ^{13}C NMR (DMSO-d6, δ ppm): 30.38 (2CH_3), 40.50 (CH_2), 115.58, 116.69, 124.29, 127.90, 128.57, 131.20 (Ar-C), 154.07, 154.18, 168.63 (3C=O), MS, *m*/*z* (%): 362 [M + 2]$^+$ (14.42), 360 [M$^+$] (32.07), analysis for $C_{12}H_{13}ClN_4O_5S$ (360.77), calcd% C, 39.95; H, 3.63; Cl, 9.83; N, 15.53; S, 8.89, found: % C, 40.17; H, 3.82; Cl, 9.72; N, 15.65; S, 9.03.

*2.1.4.3. N′-Benzoyl-1,4-dimethyl-2,3-dioxo-1,2,3,4-tetrahydroquinoxaline-6-sulfonohydrazide (**9c**).* Yield (70%), mp. 136–138 °C, IR (ν_{max}/cm^{-1}): 3433, 3234 (2NH), 3006 (CH, aromatic), 2931 (CH-alicyclic), 1670, 1663 (3C=O), 1291, 1178 (SO_2), ^{1}H NMR (DMSO-d_6, δ ppm): 3.50, 3.57 (2s, 6H, 2CH_3), 7.22–7.27 (m, 3H, aromatic-H), 7.45 (d, 2H, aromatic-H, J = 6.00 Hz), 7.55, 7.67 (2d, 2H, aromatic-H, J = 5.67 Hz), 7.76 (s, 1H, aromatic-H), 9.16, 10.03 (2s, 2H, 2NH, exchangeable with D_2O), ^{13}C NMR (DMSO-d$_6$, δ ppm): 30.38 (2CH_3), 114.59, 115.57, 115.82, 116.71, 123.51, 124.30, 127.78, 127.89, 128.55, 131.26, 134.29 (Ar–C), 154.08, 154.34, 168.63 (3C=O), MS, *m*/*z* (%): 388 [M]$^+$ 36.07, analysis for $C_{17}H_{16}N_4O_5S$ (388.40), calcd% C, 52.57; H, 4.15; N, 14.43; S, 8.26, found: % C, 52.85; H, 4.40; N, 14.50; S, 8.30.

2.1.5. General method for the preparation of 2-(1,4-dimethyl-2,3-dioxo-1,2,3,4-tetrahydroquinoxalin-6-ylsulfonyl)-N-substituted hydrazinecarbox(thio)amide (10a–h). To a solution of the sulfonohydrazide derivative **8** (10 mmol, 2.84 g) in DMF (20 mL) containing a few drops of triethylamine (10 mmol), the appropriate iso/isothiocyanate was added and the reaction mixture was refluxed for 6 h. After completion of the reaction, it was poured onto ice/H_2O and neutralized with HCl. The formed precipitate was collected by filtration, washed several times with water, and crystallized from the proper solvent.

*2.1.5.1. 2-(1,4-Dimethyl-2,3-dioxo-1,2,3,4-tetrahydroquinoxalin-6-ylsulfonyl)-N-isopropyl hydrazine-1-carboxamide (**10a**).* Yield (72%), crystallized from isopropanol, m.p. 290–292 °C, IR (ν_{max}/cm^{-1}): 3434, 3235, 3108 (3NH), 3058 (CH, aromatic), 2930 (CH-alicyclic), 1675, 1663 (3C=O), 1380, 1157 (SO_2), ^{1}H NMR (DMSO-d_6, δ ppm): 1.09 (d, 6H, 2CH_3-isopropyl, J = 6.40 Hz), 3.40 (s, s, 6H, 2CH_3), 4.26 (m, 1H, CH-isopropyl), 5.46 (s, 1H, 1NH, exchangeable with D_2O), 7.40–7.51 (m, 3H, aromatic-H), 7.91 (s, 2H, 2NH, exchangeable with D_2O), ^{13}C NMR (DMSO-d_6, δ ppm): 23.42, 30.36 (4CH_3), 45.70 (CH_2), 123.03, 125.26, 127.46, 131.21, 135.47 (Ar–C), 156.07, 158.57 (3C=O), MS, *m*/*z* (%): 370 [M$^+$ + 1] (33.53) 369 [M$^+$] (24.39), analysis for $C_{14}H_{19}N_5O_5S$ (369.40), calcd% C, 45.52; H, 5.18; N, 18.96; S, 8.68, found: % C, 45.63; H, 5.36; N, 18.98; S, 8.79.

*2.1.5.2. N-Benzyl-2-((1,4-dimethyl-2,3-dioxo-1,2,3,4-tetrahydroquinoxalin-6-yl)sulfonyl)hydrazine-1-carboxamide (**10b**).* Yield 73%, crystallized from ethanol, m.p. 154–156 °C, IR (ν_{max}/cm^{-1}): 3477, 3323, 3240 (3NH), 3030 (CH, aromatic), 2919 (CH-alicyclic), 1671, 1658 (3C=O), 1358, 1157 (SO_2), ^{1}H NMR (DMSO-d_6, δ ppm): 3.48 (s, 6H, 2CH_3), 4.20 (s, 2H, CH_2), 6.38 (m, 2H, 2NH, D_2O exchangeable), 7.18–7.30 (m, 8H, aromatic-H), 7.42 (s, 1H, NH, exchangeable with D_2O), ^{13}C NMR (DMSO-d$_6$, δ ppm): 30.36 (2CH_3), 43.46 (CH_2), 115.61, 116.68, 124.29, 127.01, 127.46, 128.67, 131.21, 141.36, 154.07, 154.17 (Ar–C), 158.57, 165.41 (3C=O), MS, *m*/*z* (%): 417 [M$^+$] (23.58), analysis for $C_{18}H_{19}N_5O_5S$ (417.44), calcd % C, 51.79; H, 4.59; N, 16.78; S, 7.68, found: % C, 51.85; H, 4.73; N, 16.83; S, 7.83.

*2.1.5.3. N-Benzoyl-2-((1,4-dimethyl-2,3-dioxo-1,2,3,4-tetrahydroquinoxalin-6-yl)sulfonyl)hydrazine-1-carboxamide (**10c**).* Yield (75%), crystallized from ethanol, m.p. 290–292 °C, IR (ν_{max}/cm^{-1}): 3562, 3490, 3474 (3NH), 3058 (CH, aromatic), 2928

(CH-alicyclic), 1675, 1670, 1650 (4C=O), 1253, 1159 (SO_2), ^{1}H NMR (DMSO-d_6, δ ppm): 3.47 (s, 6H, $2CH_3$), 7.32 (s, 1H, NH, exchangeable with D_2O), 7.41–7.52–7.66 (m, 8H, aromatic-H, 1H, NH), 8.11 (s, 1H, NH, exchangeable with D_2O), ^{13}C NMR (DMSO-d_6, δ ppm): 30.33 ($2CH_3$), 115.52, 116.31, 116.61, 124.23, 127.83, 128.49, 128.78, 129.09, 131.23, 132.12, 133.27, 153.73 (Ar–C), 156.45, 165.41 (4C=O), MS, *m/z* (%): 431 [M^+] (32.58), analysis for $C_{18}H_{17}N_5O_6S$ (431.42), calcd % C, 50.11; H, 3.97; N, 16.23; S, 7.43, found: % C, 50.35; H, 4.08; N, 16.47; S, 7.66.

*2.1.5.4. N-(4-Chlorophenyl)-2-((1,4-dimethyl-2,3-dioxo-1,2,3,4-tetrahydroquinoxalin-6-yl)sulfonyl)hydrazine-1-carboxamide (**10d**).* Yield (75%), crystallized from isopropanol/pet. ether, m.p. 260–262 °C, IR (ν_{max}/cm^{-1}): 3433, 3390, 3360 (3NH), 3058 (CH, aromatic), 2920 (CH-alicyclic), 1671, 1653 (3C=O), 1253, 1159 (SO_2), ^{1}H NMR (DMSO-d_6, δ ppm): 3.44 (s, 6H, $2CH_3$), 5.75, 5.90 (2s, 2H, 2NH, exchangeable with D_2O), 6.84–7.66 (m, 7H, aromatic-H), 8.10 (s, 1H, NH, exchangeable with D_2O), ^{13}C NMR (DMSO-d_6, δ ppm):, 30.37 ($2CH_3$), 116.78, 120.06, 122.75, 124.23, 126.93, 127.64, 128.49, 129.17, 131.23, 133.62, 140.58, 153.73 (Ar–C), 156.45, 165.58 (3C=O), MS, *m/z* (%): 437 [M^+] (28.09), analysis for $C_{17}H_{16}ClN_5O_5S$ (437.86), calcd% C, 46.63; H, 3.68; Cl, 8.10; N, 15.99; S, 7.32, found: % C, 46.85; H, 3.88; Cl, 8.27; N, 16.08; S, 7.52.

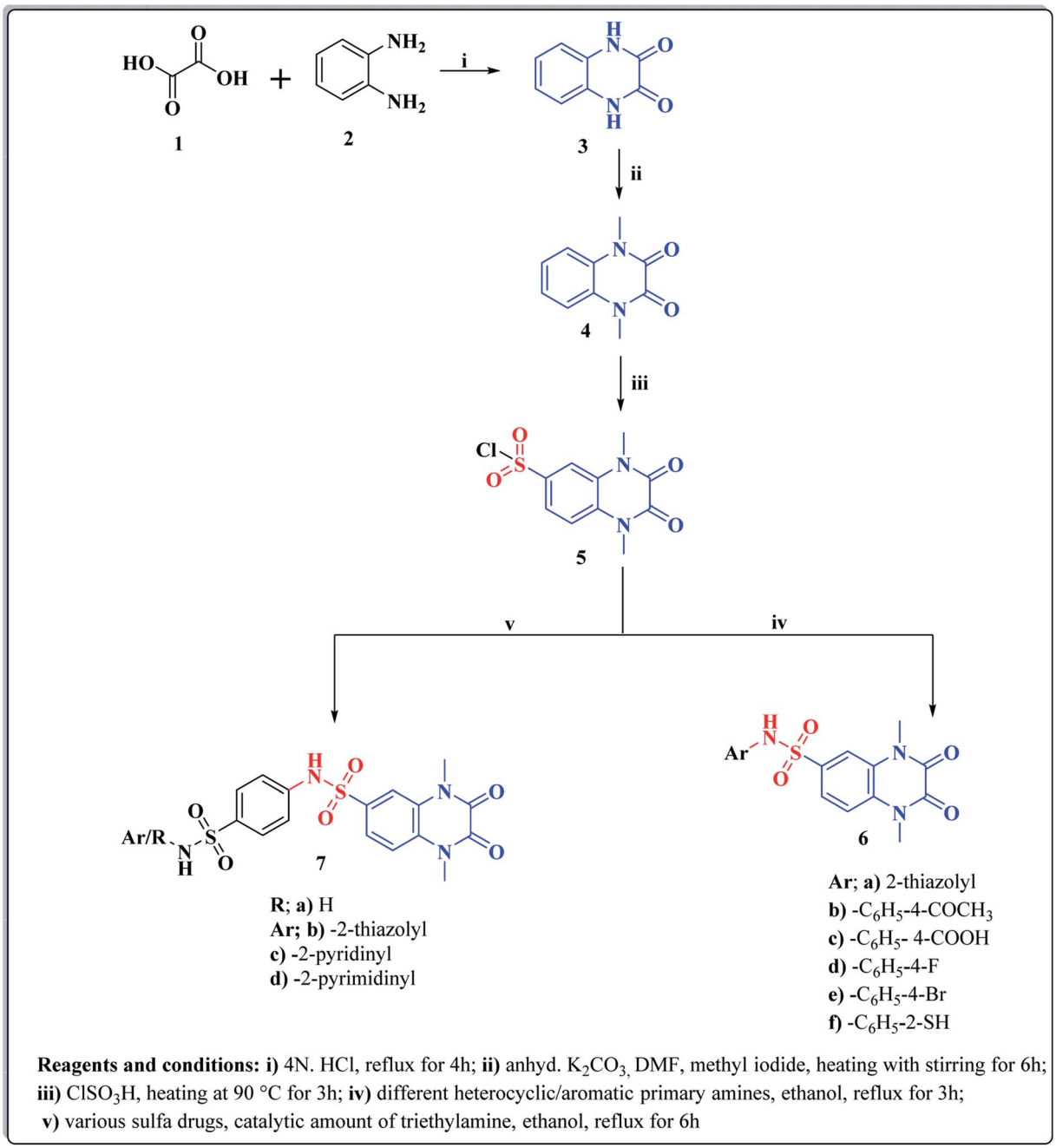

Scheme 1 Synthesis of new 1,2,3,4-tetrahydroquinoxaline-6-sulfonamide derivatives 6a–d, 7a–f.

*2.1.5.5. 2-((1,4-Dimethyl-2,3-dioxo-1,2,3,4-tetrahydroquinoxalin-6-yl)sulfonyl)-N-ethyl hydrazine-1-carbothioamide (**10e**).* Yield (73%), crystallized from ethanol, m.p. 124–126 °C, IR (ν_{max}/cm^{-1}): 3454, 3367, 3360 (3NH), 3065 (CH, aromatic), 2933 (CH-alicyclic), 1677 (2C=O), 1456 (C=S), 1253, 1159 (SO_2), ^{1}H NMR (DMSO-d_6, δ ppm): 1.15 (t, 3H, CH_3, J = 5.5 Hz), 3.44 (s, 6H, $2CH_3$), 3.63 (q, 2H, CH_2, J = 5.5 Hz), 7.24–7.38 (m, 3H, aromatic-H), 7.48, 7.60, 7.91 (3s, 3H, 3NH, exchangeable with D_2O), ^{13}C NMR (DMSO-*d6*, δ ppm): 16.28, 30.33 ($3CH_3$), 41.37 (CH_2), 122.38, 127.25, 128.49, 131.23, 133.57 (Ar–C), 154.58 (2CO), 180.05 (C=S), MS, *m*/*z* (%): 373 [M + 2]$^+$ (35.83), 371 [M$^+$] (30.26), analysis for $C_{13}H_{17}N_5O_4S_2$ (371.44), calcd% C, 42.04; H, 4.61; N, 18.85; S, 17.27, found: % C, 42.17; H, 4.86; N, 18.67; S, 17.39.

*2.1.5.6. N-Cyclohexyl-2-((1,4-dimethyl-2,3-dioxo-1,2,3,4-tetrahydroquinoxalin-6-yl)sulfonyl)hydrazine-1-carbothioamide (**10f**).* Yield (70%), crystallized from isopropanol/pet. ether, m.p. 151–153 °C, IR (ν_{max}/cm^{-1}): 3473, 3387, 3350 (3NH), 3076 (CH, aromatic), 2927 (CH-alicyclic), 1672 (2C=O), 1458 (C=S), 1328, 1156 (SO_2), ^{1}H NMR (DMSO-d_6, δ ppm): 1.10–1.18 (m, 2H, CH_2-cyclohexyl), 1.40–1.59 (m, 4H, $2CH_2$-cyclohexyl), 1.61–1.78 (m, 4H, $2CH_2$-cyclohexyl), 3.08–3.18 (m, 1H, CH-cyclohexyl), 3.46 (s, 6H, $2CH_3$), 6.60, 6.81 (2s, 3H, 3NH, exchangeable with D_2O), 7.04–7.06, 7.39–7.50 (2m, 2H, aromatic-H), 7.61 (s, 1H, aromatic-H), ^{13}C NMR (DMSO-*d6*, δ ppm): 24.52 ($3CH_2$), 30.33 ($2CH_3$), 35.08 ($2CH_2$), 56.72 (CH), 121.28, 125.46, 128.49, 133.25, 133.82 (Ar–C), 155.64 (2CO), 183.26 (C=S), MS, *m*/*z* (%): 427 [M + 2]$^+$ (35.83), 425 [M$^+$] (30.26), analysis for $C_{17}H_{23}N_5O_4S_2$ (425.53), calcd% C, 47.98; H, 5.45; N, 16.46; S, 15.07, found: % C, 48.07; H, 5.74; N, 16.83; S, 15.32.

*2.1.5.7. 2-((1,4-Dimethyl-2,3-dioxo-1,2,3,4-tetrahydroquinoxalin-6-yl)sulfonyl)-N-phenyl hydrazine-1-carbothioamide (**10g**).* Yield (77%), crystallized from isopropanol, m.p. 100–102 °C. IR (ν_{max}/cm^{-1}): 3426, 3345, 3230 (3NH), 3058 (CH, aromatic), 2928 (CH-alicyclic), 1671 (2C=O), 1451 (C=S), 1317, 1158 (SO_2), ^{1}H NMR (DMSO-d_6, δ ppm): 3.44 (s, 6H, $2CH_3$), 5.95, 6.12 (2s, 2H, 2NH, exchangeable with D_2O), 6.85–7.48 (m, 8H, aromatic-H), 8.04 (s, 1H, NH, exchangeable with D_2O), ^{13}C NMR (DMSO-d_6, δ ppm):, 30.37 ($2CH_3$), 118.30, 121.34, 122.47, 123.59, 125.46, 126.28, 128.73, 130.28, 133.25, 138.27 (Ar–C), 157.08 (2CO), 185.24 (C=S). MS, *m*/*z* (%): 419 [M$^+$] (34.27), analysis for $C_{17}H_{17}N_5O_4S_2$ (419.47), calcd % C, 48.68; H, 4.08; N, 16.70; S, 15.29, found: % C, 48.85; H, 3.88; N, 16.79; S, 15.53.

*2.1.5.8. 2-((1,4-Dimethyl-2,3-dioxo-1,2,3,4-tetrahydroquinoxalin-6-yl)sulfonyl)-N-(4-methoxyphenyl)hydrazine-1-carbothioamide (**10h**).* Yield (75%), crystallized from ethyl-acetate, m.p. 136–138 °C. IR (ν_{max}/cm^{-1}): 3433, 3345, 3234 (3NH), 3006 (CH, aromatic), 2931 (CH-alicyclic), 1671 (2C=O), 1458 (C=S), 1291, 1178 (SO_2). ^{1}H NMR (DMSO-d_6, δ ppm): 3.53 (s, 6H, $2CH_3$), 3.70 (s, 3H, OCH_3), 6.84, 6.92 (2d, 4H, aromatic-H, J = 10.01 Hz), 7.20–7.28 (m, 3H, aromatic-H), 7.44, 9.44, 9.58 (3s, 3H, 3NH, exchangeable with D_2O), ^{13}C NMR (DMSO-*d6*, δ ppm):, 30.33 ($2CH_3$), 55.27 (OCH_3), 117.27, 119.30, 120.37, 126.48, 128.49, 133.25, 133.82, 142.59, 150.72, 153.30 (Ar–C), 156.48 (2CO), 185.08 (C=S), MS, *m*/*z* (%): 449 [M^{+}] (36.27), analysis for

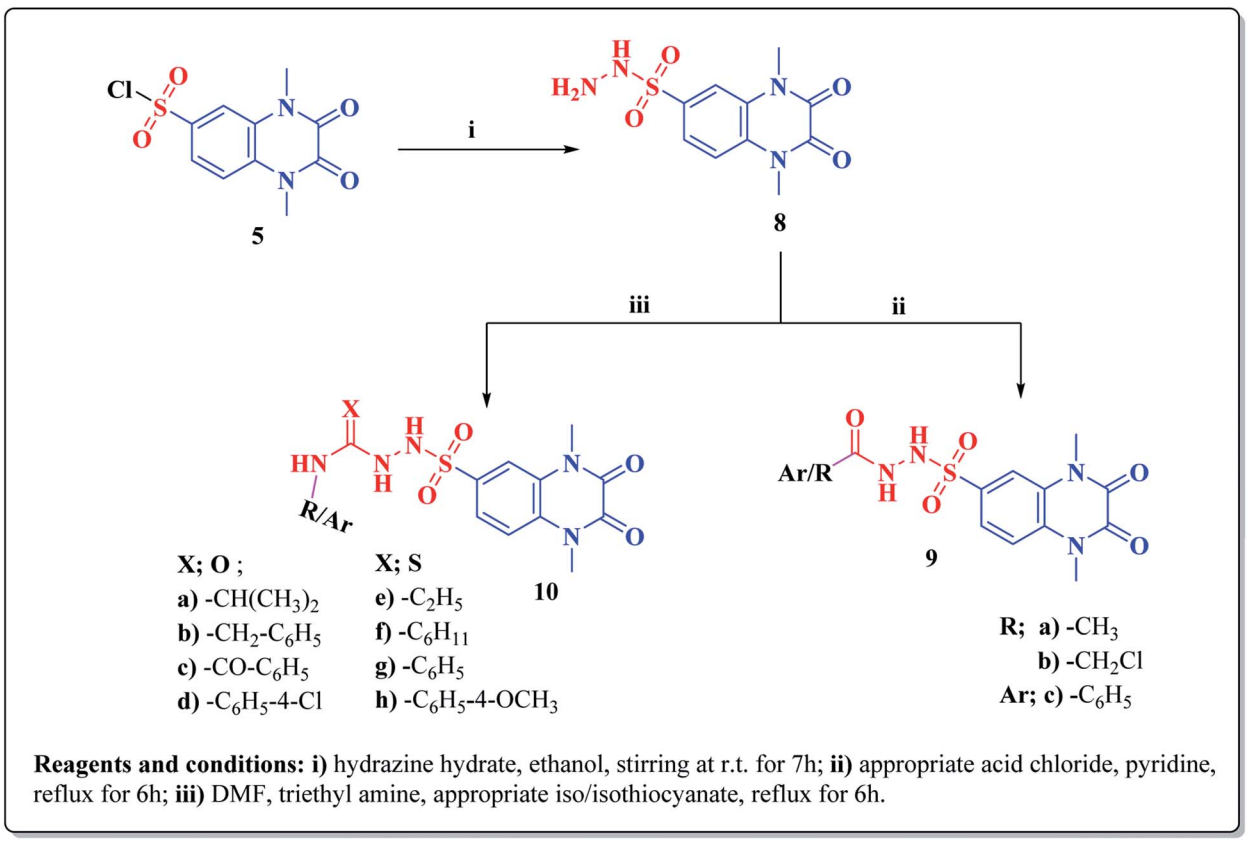

Scheme 2 Synthesis of new 1,2,3,4-tetrahydroquinoxaline-6-sulfonamide hydrazine carbox (thio)amide derivatives **9a–c**, **10a–h**.

$C_{18}H_{19}N_5O_5S_2$ (449.50), calcd% C, 48.10; H, 4.26; N, 15.58; S, 14.27, found: % C, 48.27; H, 4.36; N, 15.65; S, 14.33.

2.2. Biological studies

All of the biological data were cited in the details in the ESI† file.

2.3. Computational studies

All of the computational studies were cited in the details in the ESI† file.

2.4. Radiopharmaceutical evaluation of SQ compound

The details of the radiopharmaceutical evaluation approach were cited in the ESI† file.

3. Results and discussion

3.1. Chemistry

The synthetic approaches of the target compounds are depicted in Schemes 1 and 2. The key starting compound, quinoxaline-2,3(1*H*,4*H*)-dione (**3**), was obtained by condensation of the commercially available oxalic acid (**1**) with *o*-phenylenediamine (**2**) in alkaline medium. *N*-Alkylation of **3** with methyl iodide in the presence of anhydrous K_2CO_3 led to the formation of the corresponding 1,4-dimethyl analogue **4**.[57] Chlorosulfonation of the alkylated derivative **3** with chlorosulfonic acid led to the formation of the corresponding key 6-sulfonyl chloride intermediate **5**,[58] which was allowed to react with different heterocyclic/aromatic primary amines, namely, 2-aminothiazole, 4-aminoacetophenone, 4-aminobenzoic acid, 4-fluoroaniline, 4-bromoaniline and 2-aminothiophenol, to obtain

Table 1 DPP-4 inhibitory activity (IC_{50}; nM) of the new target compounds[a]

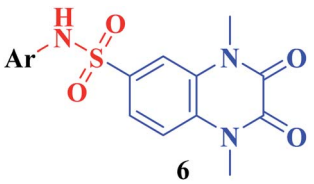

6

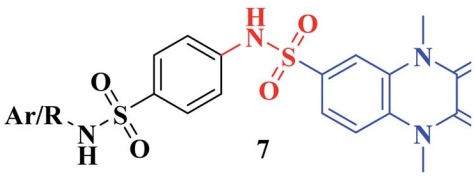

7

Compound no.	Ar=	IC_{50} (nM)
6a	–2-Thizolyl	nd
6b	$-C_6H_5$-4-$COCH_3$	1.28 ± 0.099
6c	$-C_6H_5$-4-COOH	0.74 ± 0.103
6d	$-C_6H_5$-4-F	0.70 ± 0.112
6e	$-C_6H_5$-4-Br	0.71 ± 0.075
6f	$-C_6H_5$-2-SH	0.67 ± 0.055
7a	H	0.60 ± 0.086
7b	–2-Thizolyl	0.93 ± 0.128
7c	–2-Pyridinyl	0.48 ± 0.052
7d	–2-Pyrimidinyl	0.48 ± 0.050

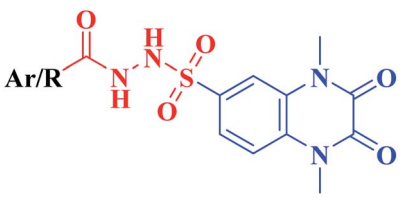

9

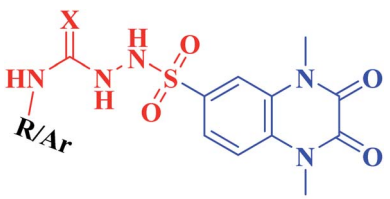

10

9a	$-CH_3$	0.085 ± 0.004
9b	$-CH_2Cl$	0.095 ± 0.006
9c	$-C_6H_5$	0.095 ± 0.012
10a	X; O, $-CH(CH_3)_2$	0.039 ± 0.042
10b	X; O, $-CH_2-C_6H_5$	0.048 ± 0.067
10c	X; O, $-CO-C_6H_5$	0.144 ± 0.107
10d	X; O; C_6H_5-4-Cl	nd
10e	X; S, $-C_2H_5$	0.068 ± 0.044
10f	X; S, $-C_6H_{11}$	0.055 ± 0.110
10g	X; S, $-C_6H_5$	0.049 ± 0.031
10h	X; S, $-C_6H_5$-4-OCH_3	nd
STZ-C		
Linagliptin		0.77 ± 0.0085

[a] STZ-C: diabetic control.

the corresponding sulfonamide compounds **6a–f**, respectively. Furthermore, compound **5** was treated with various sulfa drugs, namely, sulfanilamide, sulfathiazole, sulfapyridine and sulfadiazine in ethanol containing a catalytic amount of triethylamine, to afford the corresponding sulfa derivatives **7a–d**, respectively (Scheme 1).

Furthermore, hydrazinolysis of the 6-sulfonyl chloride intermediate **5** was carried out by its treatment with hydrazine hydrate in ethanol to get the corresponding 6-sulfonohydrazide derivative **8**, which in turn underwent nucleophilic substitution by its reaction with various acid chloride derivatives, namely, acetyl chloride, 2-chloroacetyl chloride and benzoyl chloride, as well as with different iso(thio)cyanates to accomplish the corresponding N-substituted-6-sulfonohydrazide and hydrazinecarbox(thio)amide derivatives **9a–c**, **10a–h**, respectively (Scheme 2). The structural identification of the new target compounds was performed by microanalytical and IR, ^{1}H NMR, ^{13}C NMR and mass spectral data, which were in conformity with their assigned molecular structures. IR spectra exhibited absorption bands in the range of 3344–3174 cm^{-1} related to the NH groups, 1710–1653 cm^{-1} assigned to the 2C=O$_{quinoxaline}$ groups, in addition to two bands in the range 1388–1134 cm^{-1} representing the SO_2 groups. The compounds **6b**, **6c**, **9a–c** and **10a–d** represented the additional absorption bands at 1710–1653 cm^{-1}, confirming the presence of the acetyl, carboxylic and carboxamide C=O groups, respectively, while compounds **10e–h** revealed absorption bands at the region of 1458–1451 cm^{-1} related to the C=S functionality. Furthermore, the ^{1}H NMR data displayed a singlet signal at δ 3.40–3.50 ppm integrating the six protons of the 1,4-di-CH_3 groups and a singlet D_2O exchangeable signal at the range of δ 5.92–6.70 ppm due to the sulfonamide NH groups, while the aromatic protons appeared at their expected regions. The compounds **6b**, **6c**, **6f** exhibited additional singlets at δ 3.08, 10.08, 5.41 ppm attributed to CH_3, OH and SH, respectively. On the other hand, the aromatic zone of compounds **7a–d** integrated higher proton numbers attributed to the conjugated phenylsulfonamide moieties. Moreover, the acetyl and benzyl sulfonamide compounds **9a**, **9b** displayed two singlets at δ 2.05 and 4.21 ppm integrated for –COC*H*$_3$ and ph-CH_2 protons. In contrast, the hydrazinecarboxamide derivative **10a** exhibited an up-field doublet signal resonating at δ 1.09 ppm due to the 2CH_3-isopropyl. Meanwhile, the methine CH-isopropyl appeared as a multiplet signal at δ 4.32 ppm, in addition to three D_2O exchangeable singlets at δ 5.53–5.60 and 7.91 ppm related to the 3NH groups. Furthermore, besides the parent protons at the expected zones, compounds **10b**, **10e**, **10h** exhibited a singlet signal at δ 4.20 ppm, characteristic triblet-quartet signals at δ 1.15, 3.63 ppm and a singlet signal at δ 3.70 ppm attributed to the ph-CH_2, –CH_2–CH_3 and –OCH_3 groups, respectively. Furthermore, the cyclohexyl protons of compound **10f** were represented as three upfield multiplets at δ 1.10–1.14, 1.65–1.78, 3.08–3.11 ppm, attributed to 3CH_2-α, 2CH_2-β and CH, respectively. ^{13}C NMR spectra of the target compounds showed singlet signals at the regions of δ 30.30–30.45, 158.87–165.41 characterizing the parent quinoxaline-1,3-dimethyl, as well as 2,3-dioxo groups. In addition, other signals appeared by compounds **6b** at δ 30.21 ppm, **10a** at δ 23.11, 24.12, 52.0 ppm, **10b** at δ 43.46 ppm, **10e** at δ 16.42, 39.79 ppm, **10f** at δ 25.32, 30.60, 60.41 ppm and **10h** at δ 55.67 ppm, characterized as –COC*H*$_3$, –CH(CH_3)$_2$, –*C*H_2-ph, –C_2H_5, –C_6H_{11}, and –OCH_3, respectively.

3.2. Biological studies

3.2.1. *In vitro* DPP-4 and DPP-8/9 assay. The new target compounds **6**, **7**, **9**, and **10** were evaluated as *in vitro* DPP-4 inhibitors taking Linagliptin as a reference drug, according to

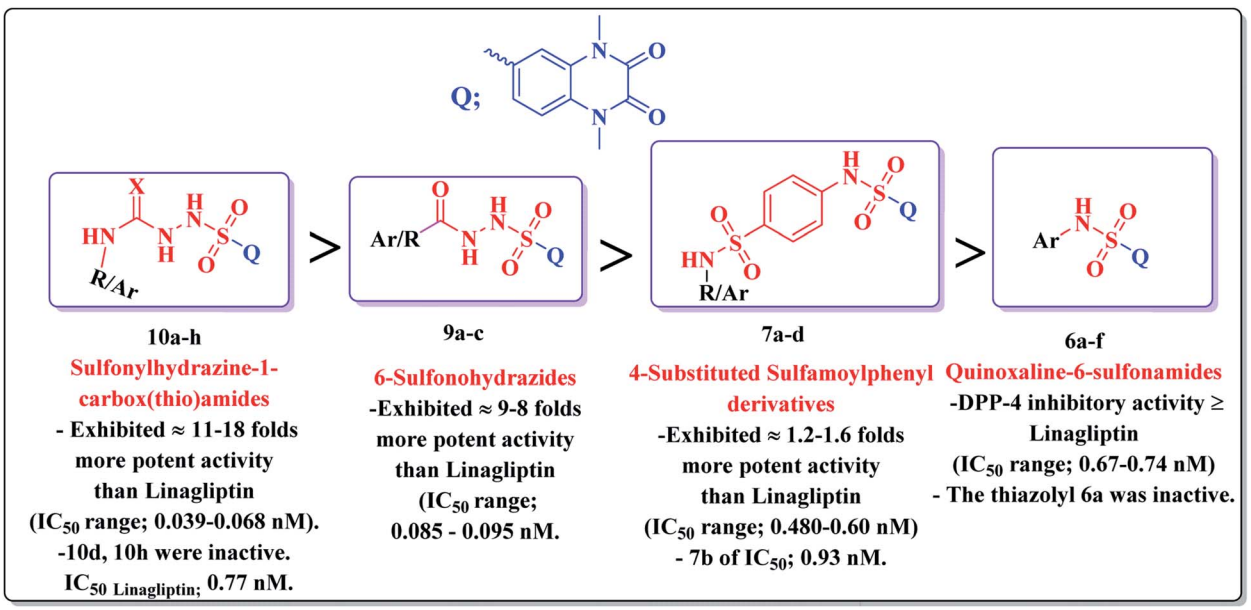

Fig. 4 Structure activity relationship analyses of the resultant data of DPP-4 inhibitory assessment.

Table 2 DPP-8 and DPP-9 inhibition activity of compounds **7d**, **9a**, **10a**, **10g**

Compound no.	DPP-8 (μM)	DPP-9 (μM)
7d	>100	>100
9a	>100	>100
10a	>100	>100
10g	>100	>100

the previously reported method.[50] The obtained results are expressed as IC_{50} (nM) and summarized in Table 1.

It could be noted that most of the tested derivatives produced a promising DPP-4 suppression effect, indicating that the quinoxaline-6-sulfonamide scaffold is pivotal for the DPP-4 inhibitory potency. Structure activity relationship analyses revealed the following points:

• Conjugation of the 2,3-dioxo-1,2,3,4-tetrahydroquinoxaline motif with various substituted aromatic moieties *via* the 6-sulfonamide linker as compounds **6b–f** exhibited DPP-4 inhibitory activity that was approximately equipotent or slightly less than that obtained by the reference drug Linagliptin of IC_{50} values ranging from 0.67–1.28 nM, $IC_{50Linagliptin}$; 0.77 nM, while the suppression activity was completely lost by the thiazolyl derivative **6a**.

• On the other hand, conjugation of the parent 2,3-dioxo-1,2,3,4-tetrahydro quinoxaline-6-sulfonamide with different 4-(heterocyclic) sulfamoylphenyl moieties as compounds **7** led to a significant influence on inhibitory activity. The 4-sulfamoylphenyl, the pyridinyl and the pyrimidinyl analogues **7a**, **c**, **d** represented 1.2–1.6 folds more potent DPP-4 inhibitory effect than that obtained by Linagliptin of IC_{50}s; 0.60, 0.48 and 0.48 nM, respectively. The presence of an additional sulfamoyl functionality might be the reason for enhancement of the suppression effect of the latter ligands by forming extra hydrogen bonds with the active pocket of DPP-4. A slight decrease in the potency was detected by the thiazolyl derivative **7b** of IC_{50}; 0.93 nM.

• Furthermore, the resultant data showed that the elongation of the 6-sulfonamide linker to 6-sulfonohydrazide leading to the formation of the ligands **9a–c** produced a robust influence on the inhibitory activity. The compounds **9a–c** exhibited a DPP-4 suppression effect that was about **8–9** folds more potent than Linagliptin (IC_{50}; 0.085, 0.095, 0.095 nM, respectively). The detected pronounced activity of **9a–c** might be explained due to the presence of additional N and O atoms acting for extra H-interaction with the active site of the target enzyme.

• Furthermore, an outstanding increase in the DPP-4 suppression potency by 11–18 folds compared to linagliptin was investigated upon prolongation of the 6-sulfonohydrazide linker to sulfonyl-N-substituted hydrazine-1-carbox(thio)amide, creating the corresponding analogues **10** of IC_{50} range 0.039–0.068 nM, a result which could be explained due to further bindings with the amino acid residues in the active pocket of the enzyme. The *p*-chlorophenyl and *p*-methoxyphenyl derivatives **10d**, **10h**, respectively, completely lost the activity. The conformation restriction of the latter ligands could explain the dramatic loss of the target activity (Fig. 4).

Subsequently, compounds **7d**, **9a**, **10a**, **10g** showing promising DPP-4 suppression activity were selected as representative examples to perform the selectivity assay over DPP-4

Table 3 IPGTT assays of the new compounds in diabetic mice (10 mg kg^{-1})

Compound no.	Blood glucose level (1 h)	Blood glucose level (2 h)	Blood glucose level (3 h)	Blood glucose level (6 h)
6b	235.64 ± 4.25	127.33 ± 7.15	95.67 ± 6.21	96.24 ± 4.29
6c	220.59 ± 5.12	125.31 ± 3.47	90.68 ± 3.45	90.06 ± 7.25
6d	226.33 ± 6.34	120.08 ± 4.11	99.33 ± 1.29	93.33 ± 6.11
6e	222.09 ± 4.85	125.04 ± 3.26	95.28 ± 4.55	92.17 ± 8.45
6f	218.00 ± 4.26	118.07 ± 8.21	97.09 ± 6.39	93.25 ± 7.49
7a	251.29 ± 2.80	138.16 ± 9.23	122.08 ± 3.31	99.25 ± 4.35
7b	238.33 ± 9.27	165.66 ± 6.60	120.67 ± 7.15	95.16 ± 5.20
7c	227.37 ± 7.85	120.07 ± 8.01	97.33 ± 2.78	85.34 ± 7.16
7d	226.33 ± 4.23	117.33 ± 7.20	98.33 ± 8.11	90.31 ± 3.25
9a	237.40 ± 3.15	115.11 ± 4.25	97.12 ± 8.37	85.23 ± 1.69
9b	223.89 ± 3.85	118.12 ± 5.95	89.12 ± 4.21	85.25 ± 2.12
9c	235.40 ± 3.85	120.11 ± 2.35	96.68 ± 4.25	80.16 ± 5.01
10a	227.67 ± 3.85	110.67 ± 7.28	85.67 ± 4.89	79.33 ± 1.25
10b	228.71 ± 3.85	120.09 ± 3.35	90.66 ± 5.35	85.66 ± 4.10
10c	225.65 ± 3.85	155.33 ± 2.78	137.34 ± 9.48	104.08 ± 3.35
10e	225.33 ± 3.85	125.67 ± 7.15	95.33 ± 5.48	86.66 ± 5.49
10f	237.33 ± 3.85	127.33 ± 4.23	100.06 ± 6.29	89.66 ± 2.27
10g	225.67 ± 3.85	115.65 ± 2.85	86.33 ± 2.48	85.33 ± 5.30
STZ-C	500.33 ± 3.85	600.66 ± 7.06	600.67 ± 6.75	580.06 ± 6.10
NC	135.09 ± 3.85	120.08 ± 4.11	78.33 ± 3.95	75.36 ± 1.37
Linagliptin	220.01 ± 3.85	120.89 ± 1.76	85.11 ± 2.39	85.00 ± 5.15

[a] STZ-C: diabetic control, NC: normal control. NC; normal control, STZ-C; streptozotocin-diabetic control, values are mean ±SD, $n = 4$ in each group; statistical analysis is carried out using one way ANOVA, SPSS computer program version 8, followed by CO-stat computer program.

Table 4 Inhibition percentages of compounds **7d**, **9a**, **10a**, **10g** against normal hTERT-RPE1 cells

Compound no.	Inhibition%
7d	10%
9a	20%
10a	10%
10g	6.9%

homologues; DPP-8 and DPP-9 in the DPP-4 gene family (Table 2). The results showed that the tested compounds exhibited excellent selectivity over the DPP-4 homologues proteins. All compounds **7d**, **9a**, **10a**, **10g** exhibited IC_{50} values >100 μM against both DPP-8 and DPP-9. This result revealed that all tested compounds possessed significant selectivity towards DPP-4 inhibition of about >1000 folds over that of DPP-8/9 (Table 2).

3.2.2. Evaluation of acute hypoglycemic activity. The *in vivo* anti-hyperglycemia effects of the new compounds showing promising DPP-4 inhibition activity were evaluated by performing the intraperitoneal glucose tolerance test (IPGTT) in high-fat diet-fed/streptozotocin (HFD/STZ) induced T2DM male albino mice following the previously reported method. The blood glucose levels in (mg dl^{-1}) were measured at 1, 2, 3, and 6 hours intervals.[59,60] Table 3 summarizes the changes in blood glucose levels in the tested diabetic animals following a single dose administration of the investigated compounds. The obtained findings were in line with DPP-4 inhibition activities. The blood glucose levels were restored to more or less normal levels, with no major differences relative to the control group. The compounds **9** and **10** exhibited the most potent activity, representing glucose levels very close to those obtained by linagliptin throughout the six recorded values post doses administration (Table 3).

3.2.3. Cytotoxicity bioassay. One of the parameters that distinguishes various drugs from each other is the frequency and the severity of the side effects to the normal cells at the therapeutic doses. Accordingly, it was of interest to study the safety profile of compounds **7d**, **9a**, **10a**, and **10g** as representative examples against the normal hTERT-RPE1 cell line. The suppression percentage of the normal cells by each tested compound was determined *via* MTT[61] (Table 4). It was investigated that the tested derivatives exhibited minor cytotoxic effects of 10%, 20%, 10%, and 6.9% on the examined normal cells, representing the promising safety profile of the tested compounds.

4. Computational studies

4.1. Molecular docking analysis

The compounds **9a**, **10a**, **10f**, and **10g** were selected as representative examples for the most promising compounds to carry

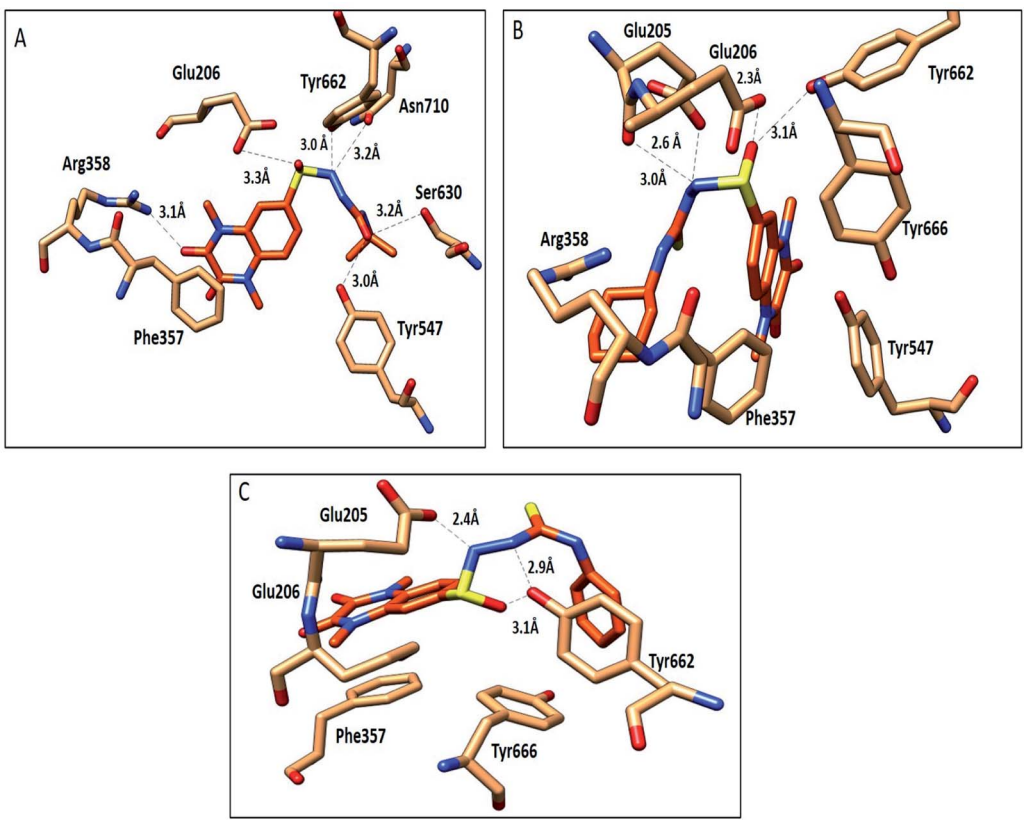

Fig. 5 Interactions of compounds **10a**, **10f** and **10g** (orange, stick) within the DPP-IV active site (PDB: 3WQA); residues represented as (sandy brown, stick). (A) Compound **10a**, (B) compound **10f**, (C) compound **10g**. H-bonds were represented as black dotted lines.

Table 5 Results of the molecular modelling study of compounds **9a**, **10a**, **10f** and **10g** within the binding active site

Compd no.	Interacting moiety in compound	Amino acid involved	Distance Å	Type of interaction
9a	S═O	NH_2 Arg125	2.5	H-Bond
	C═O	OH Ser209	2.7	H-Bond
	S═O	OH Tyr547	3.0	H-Bond
	C═O	OH Ser630	2.5	H-Bond
	NH quinoxaline moiety	N His740	3.1	H-Bond
		Phe357		π–π stacking
10a	C═O	NH Arg358	3.1	H-Bond
	C═O	OH Tyr547	3.0	H-Bond
	S═O	OH Ser630	3.2	H-Bond
	NH	OH Glu206	3.3	H-Bond
	Quinoxaline moiety	C═O Asn710	3.2	H-Bond
		OH Tyr662	3.0	H-Bond
		Phe357		π–π stacking
10f	NH	C═O Glu205	2.6	H-Bond
	S═O	C═O Glu206	2.3	H-Bond
	Quinoxaline moiety	OH Tyr662	3.1	H-Bond
		Phe357		π–π stacking
10g	NH	C═O Glu205	2.4	H-Bond
	S═O	OH Tyr662	3.1	H-Bond
	NH quinoxaline moiety	OH Tyr662	2.9	H-Bond
		Phe357		π–π stacking

out docking studies in order to explore their modes of action on the DPP-4 enzyme. The docking studies were performed against the active site of human DPP-IV protein (PDB: 3WQH) using the MOE program.[62,63] To validate our docking protocol, the co-crystalized ligand was re-docked. The root mean square deviation (RMSD) value between the native ligand and re-docked pose was ≤1 Å, which indicated the reliability of the docking protocol. The co-crystalized ligand docking result showed

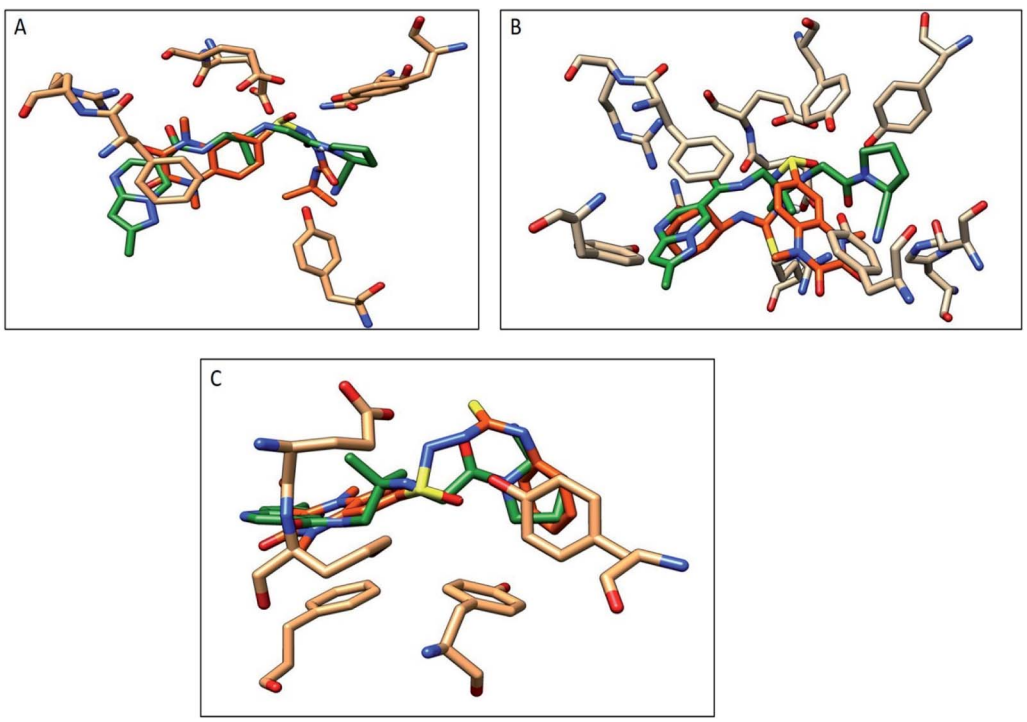

Fig. 6 Comparison of the proposed binding modes of compounds **10a**, **10f** and **10g** with co-crystalized ligand binding mode (dark green, sticks) within the DPP-IV binding pocket (PDB:3WQA). (A) Compound **10a** (orange, sticks), (B) compound **10f** (orange, sticks), (C) compound **10g** (orange, sticks).

a docking score of −4.8 kcal mol^{-1} and it formed two H-bonds between NH and Glu_205 and Glu_206 at distances 2.9 Å and 3.1 Å, respectively, and the N of the CN group formed a H-bond with Tyr547 at a distance of 3.2 Å, in addition to the π–π interactions between the phenyl group and Phen357, Tyr 585 and Tyr665.

Compound **9a** formed five H-bonds with the key residues Arg125, Ser209, Tyr547, Ser630 and His740 with a binding score of −4.9 kcal mol^{-1}. Compound **10a** showed a binding score of −5.6 kcal mol^{-1}. It formed 6 H-bonds with Glu206, Arg358, Ser630, Tyr547, Tyr662, and Asn710, while compound **10f** showed a binding score of −5.1 kcal mol^{-1} and formed four H-bonds with Glu205, Glu206 and Tyr662. The quinoxaline group of both compounds showed π–π stacking with Phe357. Furthermore, compound **10g** showed a binding score of (−7.7 kcal mol^{-1}) and illustrated three H-bonds with Glu205 and Tyr662 at a distance of (2.4, 2.9, and 3.1 Å), respectively, besides the π–π interactions between the quinoxaline group and Phe357 (Fig. 5, Table 5). Compound **10a** showed a good binding mode within the active site of DPP-IV in comparison to the co-crystallized ligand. The isopropyl amide moiety of **10a** occupied the position of acetyl pyrrolidine carbonitrile moiety of the native ligand. Meanwhile, the di-methyl quinoxalinedione moiety occupied the position of the open chain of **10a**, which links the 2-methylpyrazolo[1,5-*a*]pyrimidine with the pyrrolidine group. Replacement of the isopropyl amide group of **10a** with the cyclohexyl thioamide group **10f** showed a different binding mode. The quinoxaline moiety moved away from the position of the native ligand and protruded out of the binding pocket, and this may explain the slight decrease in the activity of **10f** (Fig. 6). Replacement of the cyclohexyl moiety in **10f** with a phenyl group as compound **10g** showed the good binding mode of **10g** (Fig. 6). The phenyl group occupied the position of the pyrrolidine of the native ligand, and the quinoxaline group occupied the position of pyrazolopyrimidine. The promising activity of **10g** may be attributed to its good binding mode within the binding site.

In conclusion, **9a**, **10a**, **10f** and **10g** showed good H-bonds profile with the key residues as Glu205, Glu206 and Tyr662, while compound **10g** with a phenyl substituent showed the best binding mode with the active site of the target protein, and this explains its good binding score and good inhibitory activity.

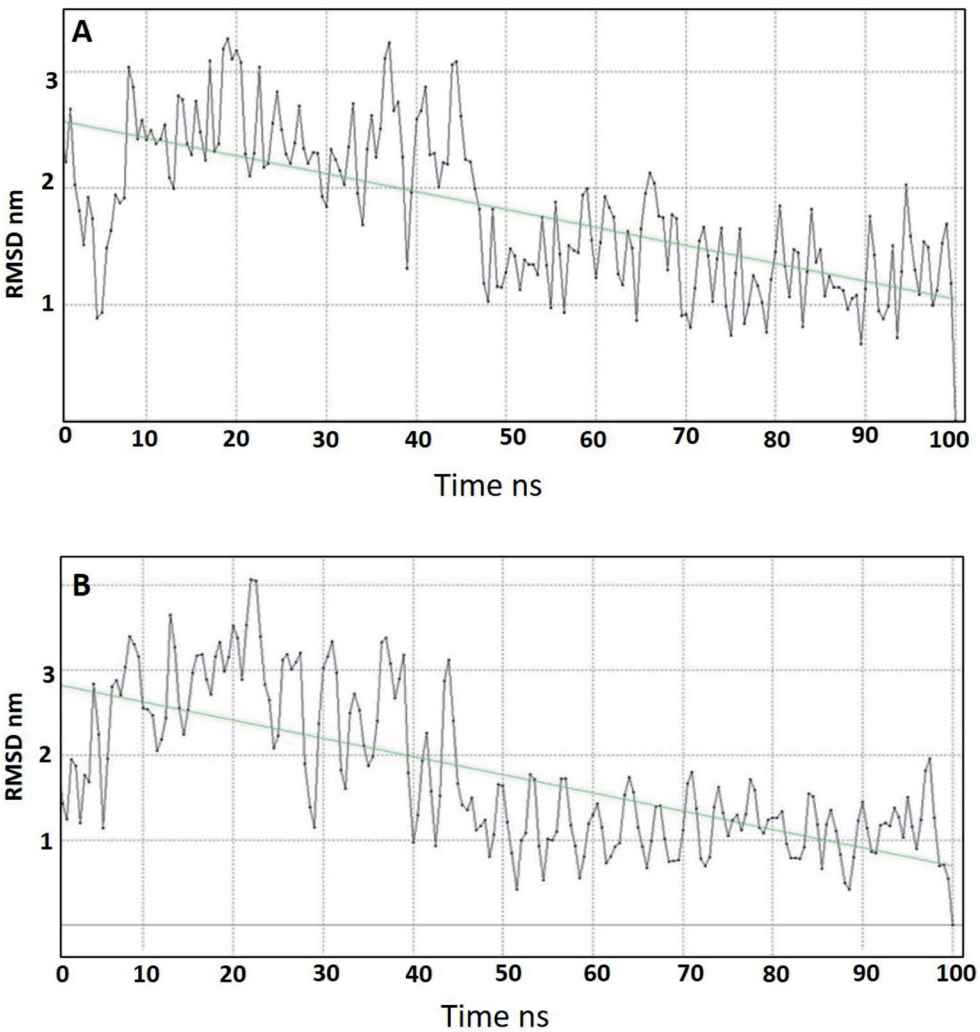

Fig. 7 RMSD of (A) compound **10a**, (B) compound **10g** over 100 ns MD simulation.

4.2. Molecular dynamics (MD) studies

Molecular dynamics studies (MD) were carried out for two of the most promising compounds **10a** and **10g** as representative examples in order to study their stability within the active site of DPP-IV.[64] The ligand–receptor complexes of **10a** and **10g** that came out from the docking simulation were used in the molecular dynamic simulation for 100 ns. Compound **10a** showed a smooth root mean square deviation (RMSD), which indicated its stability within the binding pocket. In addition, it could be seen that **10a** had two conformations over the MD simulation. The first conformation showed RMSD around 2.5 Å, and the second conformation appeared at 50 ns and showed an RMSD around 1.5 Å (Fig. 7A). Compound **10g** showed a smooth RMSD curve and two conformations (Fig. 7B). The first one showed a root mean square deviation (RMSD) of 2.5 Å and extended from 1 ns to 50 ns, while another conformation extended from 50 ns to 100 ns, illustrating an RMSD around 1.5 Å. The MD simulation results for compounds **10a**, **10g** showed nearly the same pattern, and this might be attributed to the similarity in the structures.

In conclusion, MD of compounds **10a** and **10g** showed that both compounds are stable over the MD simulation. These results explained the activity of **10a** and **10g**, which might be attributed to their stability within the active site.

4.3. Pharmacophore modelling

A molecular modelling experiment was performed to develop a hypothetical pharmacophore model for the anti-DPP-IV activity. In order to study the fitting of the designed compounds to the developed pharmacophore, a ligand-based pharmacophore model was developed using a training set of nine of diverse chemical structures that showed promising IC_{50} values. The hypothetical pharmacophore features used are the hydrogen bond donor (HBD), hydrogen bond acceptor (HBA), ring aromatic (RA) and hydrophobic aromatic feature (HAR).

4.4. Pharmacophore results

Sixteen pharmacophore models were generated *via* flexible aligning of the represented training set, and all of the pharmacophore models included at least three chemical features. The top pharmacophore model generated showed 6 features: two HBD, two HBA, one HYP, and one RA feature, as represented in Fig. 8, with constraint distances and angles between its features listed in Table 5. The top pharmacophore was selected upon the total mutual similarity score of the molecules (S) and the alignment score of the molecules (F). The top pharmacophore model was generated upon alignment molecules that showed the lowest F and S, as the lower values indicate greater similarity and better alignment. Fitting of the designed active compounds, for example, **10g** to the pharmacophore, revealed the presence of the appropriate chemical groups superimposed on the pharmacophore features (Fig. 9). Compound **10g** superimposed with 4 features; two C=O group represented 2HBA, phenyl group represented HYP and phenyl group represented RA.

4.5. QSAR studies

The QSAR study was performed to investigate the correlation between the biological activity and physicochemical properties of the training set using MOE software. The 18 compounds that showed activity against DPP-IV were selected as the training set, while inactive compounds (**6a**, **10d** and **10h**) were omitted from the analysis.[64,65] 2D Descriptors (including the molecular properties, surface area and volume, and topological descriptors) and 3D descriptors, as well as the energies of the highest occupied and the lowest unoccupied molecular orbitals (HOMO and LUMO) were calculated using the QSAR descriptors tool. The pIC_{50} was calculated as $pIC_{50} = -\log IC_{50}$. The partial linear regression (PLS) method was applied to search for the optimal QSAR models. The QSAR model was validated employing the leave one-out cross-validation (LOO) method, in which one compound is removed from the data set and the activity is correlated using the rest of the data set,[66] r^2 (squared correlation coefficient value), r^2 prediction (predictive squared correlation coefficient value), root mean square error (RMSE), and residuals between the predicted and the experimental activity of the test set, and the training set and *Z*-outlier score were applied to validate the QSAR model.

4.6. QSAR results

Eqn (1) represents the best performing QSAR model.

PIC_{50} = 0.01378 vsurf_Wp4 − 0.00817 vsurf_W5 + 0.68457 MNDO_HOMO + 0.00697 PEOE_VSA_4 + 15.53954.

PIC_{50} is the negative logarithmic value of the concentration required to produce 50% inhibition of DPP-IV activity. In this model, two vsurf_ descriptors (such as vsurf_W5 and vsurf_Wp4) were contributed for the activity prediction. The

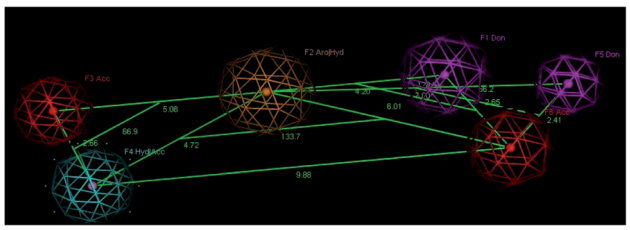

Fig. 8 Angles and constraint distances between features of the generated top pharmacophore model with the features considered to be the hydrogen bond donor (HBA) violet, hydrogen bond acceptor (HBA) red, ring aromatic (RA) brown, and hydrophobic (HYP) cyan.

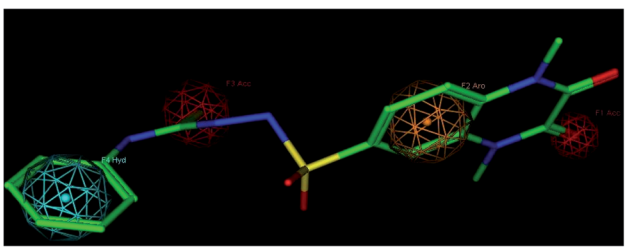

Fig. 9 Compound **10g** fitted in the pharmacophore model, hydrogen bond acceptor (HBA) red, ring aromatic (RA) brown, hydrophobic (HYP) cyan.

vsurf_descriptors are the volume and surface properties, depending on the structural connectivity of the molecules.[67] The vsurf_Wp explains the polar volume of the molecules. In general, Wp1–4 explain the polarizability and dispersion forces.[67] Here, the vsurf_Wp4 has been calculated at the _0.2 kcal mol^{-1} energy level and its positive contribution explains that the polarizable property on the van der Waals (vdW) surface of the molecules is crucial for the interactions. The vsurf_W descriptor describes the hydrophilic region of the molecules, and W5–8 accounts for the polar and hydrogen bond donor acceptor regions. vsurf_W5 was calculated at −0.3 kcal mol^{-1} energy level and the negative sign indicates that the molecules should not have many hydrogen-bond donor or acceptor groups. PEOE_VSA_4 is a partial charge descriptor. This descriptor depends on calculating the partial charge of each atom. PEOE is the Partial Equalization of Orbital Electronegativity, which is a method of calculating the atomic partial charges. Meanwhile, PEOE-VSA-4 describes the partial negative charge of the vdW surface area, and its positive charge reveals the presence of partial negative charge on the molecules, which is important. MNDO_HOMO is the energy (eV) of the Highest Occupied Molecular Orbital and its positive sign is important for the biological activity. According to eqn (1), the QSAR model is illustrated graphically by scattering plots of the experimental *versus* the predicted bioactivity, as shown in Fig. 10. The method used to build the models was partial least-squares, $r^2 = 0.7$, r^2 (pred) 0.2. r^2 (pred) is equivalent to q^2 from a leave-1-out cross-validation root mean square error (RMSE) = 0.09, cross validated RMSE = 0.17. From eqn (1), it could be concluded that the anti DPP-4 inhibition activity of the training set increased by increasing vsurf_Wp4, PEOE_VAS_4 and MANDO_H, while it increased by decreasing vsurf_W5.

4.7. QSAR validation

QSAR models were evaluated internally by applying the leave-one-out cross-validation, where r^2 (squared correlation coefficient value) is 0.7, and r^2 (pred) is 0.2. The RMSE value was so small = 009. The high value of r^2 and low value of RMSE indicate the reliability of the model. The resulting model was also validated by measuring the residuals between the experimental activity and the predicted activity of the training set (Table 7). It is notable that the difference between the predicted activity by the QSAR model is so close to the experimental activity, which is evidence of the efficacy of the model to be applied for the prediction of more effective hits. In addition, the *Z*-score was used in the model evaluation (Table 6), and there is no compound that is an outlier.

Table 6 Constraint distances and angles between features of the generated pharmacophore models

Constrains distance (Å)	Constraint angles (°)
F1–F6 2.65	F2–F3–F4 66.9
F1–F2 4.20	F6–F2–F4 133.7
F2–F3 5.08	F2–F5–F6 66.2
F3–F4 2.66	F2–F1–F6 120.9
F2–F6 6.01	
F6–F4 9.88	
F4–F2 4.72	

4.8. Drug likeness properties

In order to investigate the oral bioavailability of the best anti-DPP-IV compounds, the Lipinski's criteria of the newly synthesized compounds were calculated. Lipinski's rule is based on oral bioavailable drugs having a molecular weight (MW) of 500 or less, ten or fewer hydrogen bond acceptor sites, five or fewer hydrogen bond donor sites, and log *P* should not be greater than 5. In addition, the total polar surface area (PSA) was calculated since it is another key property that has been linked to drug bioavailability. Thus, passively absorbed molecules with

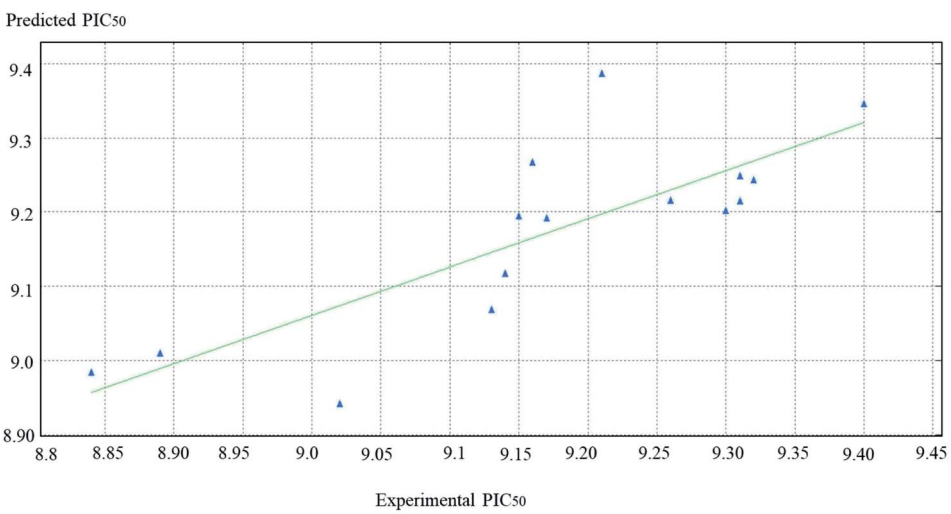

Fig. 10 The scatter plots of the experimental *versus* the predicted bioactivity values of PIC_{50} for the training set compounds.

Table 7 Experimental and predicted anti-DPP4 activity of the synthesized compounds by the QSAR model

Comp. no.	Experimental PIC_{50}	Predicted PIC_{50}	Residual	*Z*-Score
6b	8.89	9.00	−0.11	1.30
6c	9.13	9.06	0.06	0.68
6d	9.15	9.19	−0.04	0.47
6e	9.14	9.11	0.02	0.26
6f	9.17	9.19	−0.02	0.22
7a	9.21	9.38	−0.01	1.92
7b	9.02	8.94	0.07	0.87
7c	9.31	9.24	0.06	0.69
7d	9.32	9.24	0.07	0.85
9a	9.31	9.22	0.08	1.06
9b	9.03	9.01	0.09	1.07
9c	9.03	9.05	0.08	1.08
10a	9.30	9.20	0.09	1.09
10b	9.31	9.21	0.09	1.06
10c	8.84	8.98	−0.14	1.57
10e	9.16	9.26	−0.10	1.16
10f	9.26	9.21	0.04	0.50
10g	9.40	9.34	0.05	0.60

a PSA >140 Å are thought to have low oral bioavailability.[68,69] Table 8 shows that the best promising compounds **10a** and **10g** fulfilled Lipinski's rule and PSA, indicating that these promising compounds have good oral bioavailability.

5. Radiopharmaceutical evaluation of the sulfonylquinoxaline derivative **10a** (SQ) compound

5.1. Radiosynthesis of the ^{131}I-SQ compound

The derivative 2-(1,4-dimethyl-2,3-dioxo-1,2,3,4-tetrahydroquinoxalin-6-ylsulfonyl)-*N*-isopropyl hydrazine-1-carboxamide (**10a**) (SQ) was selected as a representative example for the quinoxaline derivatives to evaluate its biodistribution through *in vivo* radiolabeling the ^{131}I-SQ compound,[70–74] aiming to investigate its pharmacokinetic behavioral profile, its uptake by different body organs, alongside its elimination pathway. The radiosynthesis of the ^{131}I-SQ compound was optimized with a radiosynthesis yield after a decay correction of 94% at pH 6, 200 μg chloramine-T amount, 300 μg SQ amount, and 45 min reaction time (Fig. 11).

5.2. *In vivo* pharmacokinetic distribution of the ^{131}I-SQ compound

The results tabulated in Table 9 revealed the accumulation of the ^{131}I-SQ compound in various body organs. Interestingly, the ^{131}I-SQ compound showed high accumulation in the visceral tissues, especially the stomach and intestine, where DPP-4 is mainly released by adipose tissues and is present in a high level.[27] Thus, the examined derivative SQ (**10a**) achieved the target strategy of this study. Post-administration, it accumulates mainly in the visceral organs where DPP-4 is secreted in a high-level post prandial. This leads to the DPP-4 suppression effect,

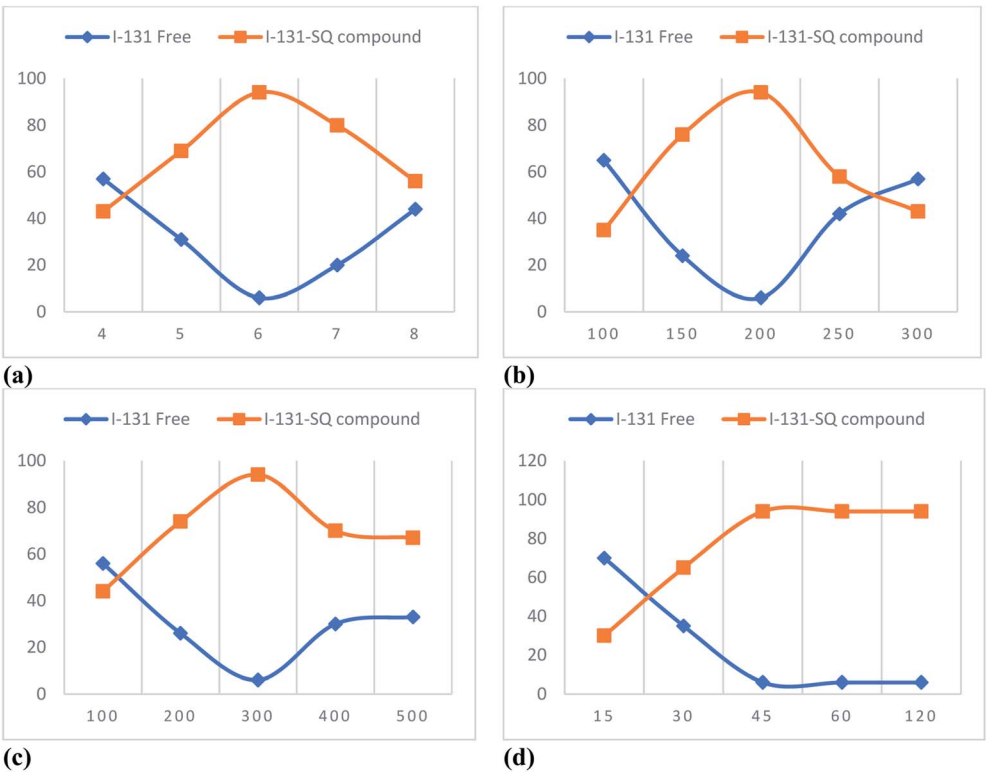

Fig. 11 Variation of % radiosynthesis yield of ^{131}I-SQ compound with (a) pH; (b) chloramine-T amount, μg; (c) SQ amount, μg; (d) reaction time, min.

Table 8 Calculated Lipinski's rule criteria of the synthesized compounds

Compd no.	M. wt	Number of HBD	Number of HBA	log *p*	log *S*	TPS (Å)
6a	352.39	1	5	0.0	−2.8	99.6
6b	387.41	1	5	0.9	−3.7	103.8
6c	389.38	3	6	0.7	−3.3	124.0
6d	389.38	3	6	0.7	−3.3	124.0
6e	424.27	1	4	1.8	−4.4	86.7
6f	377.4	1	4	1.5	−4.4	125.5
7a	424.45	2	6	−0.5	−3.6	146.9
7b	507.57	2	7	0.7	−4.5	145.8
7c	501.54	2	7	0.5	−3.7	145.8
7d	502.53	2	8	−0.5	−3.9	158.7
9a	326.33	2	5	−0.9	−2.1	115.8
9b	360.77	2	5	−0.5	−2.8	115.8
9c	388.40	2	5	0.7	−3.8	115.8
10a	369.4	3	5	−0.4	−2.6	127.9
10b	417.4	3	5	0.4	−3.7	127.9
10c	431.42	3	6	0.3	−4.1	144.9
10d	469.93	3	6	1.5	−5.7	152.1
10e	371.44	3	5	−0.5	−3.3	142.9
10f	425.53	3	5	1.0	−4.4	142.9
10g	419.48	3	5	0.8	−4.8	142.9
10h	449.51	3	6	0.8	−4.8	152.1

Table 9 *In vivo* pharmacokinetic distribution of the 131I-SQ compound

% injected dose/gm organ or body fluids					
	15 min	30 min	60 min	120 min	180 min
Blood	4.31 ± 0.51	5.00 ± 0.62	5.03 ± 0.47	4.15 ± 0.36	4.10 ± 0.55
Kidneys	5.08 ± 0.73	6.22 ± 0.87	6.76 ± 0.91	6.62 ± 0.78	5.74 ± 0.66
Liver	2.36 ± 0.21	2.65 ± 0.32	2.89 ± 0.41	3.55 ± 0.62	3.71 ± 0.73
Spleen	2.79 ± 0.19	2.20 ± 0.14	2.08 ± 0.03	3.14 ± 0.73	3.21 ± 0.44
Intestine	2.08 ± 0.26	3.18 ± 0.32	7.29 ± 1.21	5.88 ± 0.62	5.62 ± 0.69
Stomach	4.05 ± 0.63	10.58 ± 1.36	17.66 ± 1.98	20.27 ± 2.51	18.12 ± 2.34
Lungs	1.90 ± 0.09	2.18 ± 0.39	2.84 ± 0.39	2.65 ± 0.41	2.82 ± 0.24
Heart	2.04 ± 0.13	2.47 ± 0.26	2.86 ± 0.27	2.93 ± 0.30	2.87 ± 0.12
Bone	2.55 ± 0.16	2.19 ± 0.18	2.50 ± 0.22	2.60 ± 0.09	2.62 ± 0.31
Muscles	1.42 ± 0.02	1.48 ± 0.20	1.91 ± 0.07	1.44 ± 0.08	1.51 ± 0.07

blocking the inactivation of the incretin hormones with the consequent stimulation of insulin secretion and inhibition of glucagon secretion, leading to the control of the glucose level in the body.[75–83] In addition, it was clear that the excretion pathway of the ^{131}I-SQ compound is through the renal route. Moreover, it did not show any high accumulation in other body organs.

6. Conclusion

As an effort to achieve new more potent and safer antidiabetic agents, this work deals with the design and synthesis of new different derivatives bearing a quinoxaline ring system tagged with different substituted sulfonamide linkers conjugating various alkyl, heterocyclic and aromatic functionalities. All of the new ligands were evaluated as *in vitro* DPP-4 enzyme inhibitors. Most of the compounds exhibited promising suppression activity compared with Linagliptin. Compounds **7d** and **9a**, **10a**, **10g** revealed potent selectivity towards DPP-4 inhibition about >1000 folds over than DPP-8/9. Furthermore, the promising compounds were assessed as *in vivo* hypoglycemic candidates, and they exhibited promising glucose controlling effect, in comparison with linagliptin as a reference drug. Furthermore, the latter derivatives represented a promising safety profile against the healthy cells. Docking studies represented nice binding of the promising compounds **9a**, **10a**, **10g**, **10f** with the amino acid residues of the target protein DPP-4. In addition, a molecular dynamic study exhibited the stability of both **10a** and **10g** within the active site of DPP-4, which might explain their significant DPP-4 inhibiting effect. Moreover, the computational study included the creation of a hypothetical pharmacophore model for the anti-DPP-4 activity, utilizing a training set of various different chemical structures that showed promising IC_{50} values. Additionally, a QSAR study was carried out to explore the correlation between the target

suppression activity and physicochemical properties of the training set using MOE software. It has been found that the difference between the predicted activity by QSAR model is very close to the experimental one.

In addition, the pharmacokinetic pattern of compound **10a** (SQ) (selected as a representative example) was studied by radiosynthesis of the ^{131}I-SQ compound **10a**, and optimized with a radiosynthesis yield of 94% at pH 6, 200 μg chloramine-T amount, 300 μg SQ amount and 45 min reaction time. The biodistribution pattern of the tracer represented its accumulation in the visceral organs mainly in the stomach where DPP-4 is secreted in a high-level, thus inhibiting the inactivation of the incretin hormones, leading to stimulation of insulin secretion and hypoglycemic effect.

The resultant data highlighted that the quinoxaline - sulfonyl motif could provide a basic nucleus for the development of newer potent antidiabetic active hits of selective DPP-4 suppression activity of lower undesirable side effects.

Compliance with ethical standards

All animal procedures were performed in accordance with the Guidelines for Care and Use of Laboratory Animals of National Research Centre, Dokki, Giza, Egypt (NRC), and approved by the Animal Ethics Committee of The Medical Research Ethics Committee (MREC) of NRC.

Conflicts of interest

The authors declare that they have no known competing financial interests or personal relationships that could have appeared to influence the work reported in this paper.

Acknowledgements

This work was supported financially by Joint ASRT-BA Research Grants; project No. 1356 (The joint grant between the Academy of Scientific Research and Technology and Bibliotheca Alexandrina).

References

1 J. Dowarah and V. P. Singh, Anti-diabetic drugs recent approaches and advancements, *Bioorg. Med. Chem.*, 2020, **28**(5), 115263.
2 B. Bindu, S. Vijayalakshmi and A. Manikandan, Synthesis and discovery of triazolo-pyridazine-6-yl-substituted piperazines as effective anti-diabetic drugs; evaluated over dipeptidyl peptidase-4 inhibition mechanism and insulinotropic activities, *Eur. J. Med. Chem.*, 2020, **187**, 111912.
3 N. Lia, L. Wang, B. Jiang, *et al.*, Design, synthesis and biological evaluation of novel pyrimidinedione derivatives as DPP-4 inhibitors, *Bioorg. Med. Chem. Lett.*, 2018, **28**, 2131–2135.
4 J. Wang, X. Lv, J. Xu, *et al.*, Design, synthesis and biological evaluation of vincamine derivatives as potential pancreatic b-cells protective agents for the treatment of type 2 diabetes mellitus, *Eur. J. Med. Chem.*, 2020, **188**, 111976.
5 N. Li, L. Wang, Bo. Jiang, *et al.*, Recent progress of the development of dipeptidyl peptidase-inhibitors for the treatment of type 2 diabetes mellitus, *Eur. J. Med. Chem.*, 2018, **151**, 145–157.
6 Y. Zheng, S. H. Ley and F. B. Hu, Global aetiology and epidemiology of type 2 diabetes mellitus and its complications, *Nat. Rev. Endocrinol.*, 2018, **14**(2), 88–98.
7 S. E. Kahn, M. E. Cooper and S. Del Prato, Pathophysiology and treatment of type 2 diabetes: perspectives on the past, present, and future, *Lancet*, 2014, **383**(9922), 1068–1083.
8 A. B. Olokoba, O. A. Obateru and L. B. Olokoba, Type 2 diabetes mellitus: a review of current trends, *Oman Med. J.*, 2012, **27**, 269–273.
9 H. Bugger and E. D. Abel, Molecular mechanisms of diabetic cardiomyopathy, *Diabetologia*, 2014, **57**, 660–671.
10 K. Kostev and W. Rathmann, Diabetic retinopathy at diagnosis of type 2 diabetes in the UK: a database analysis, *Diabetologia*, 2013, **56**, 109–111.
11 K. Cohen, N. Shinkazh, J. Frank, I. Israel and C. Fellner, Pharmacological Treatment Of Diabetic Peripheral Neuropathy, *Physical Therapy*, 2015, **40**(6), 375–388.
12 S. Javed, I. N. Petropoulos, U. Alam and R. A. Malik, Treatment of painful diabetic neuropathy, *Ther. Adv. Chronic Dis.*, 2015, **6**(1), 15–28.
13 D. Bukleta, S. Krasniqi, G. Beretta, *et al.*, Impact of combined non-surgical and surgical periodontal treatment in patients with type 2 diabetes mellitus-a preliminary report randomized clinical study, *Biomed. Res. J.*, 2018, **29**(3), 633–639.
14 S. M.-W. Yu and J. V. Bonventre, Acute Kidney Injury and Progression of Diabetic Kidney Disease, *Adv. Chronic Kidney Dis.*, 2018, **25**(2), 166–180.
15 S. F. Spampinato, G. I. Caruso, R. D. Pasquale, M. A. Sortino and S. Merlo, The Treatment of Impaired Wound Healing in Diabetes: Looking among Old Drugs, *Pharmaceuticals*, 2020, **13**, 60.
16 A. E. Kitabchi, G. E. Umpierrez, J. N. Fisher, *et al.*, Thirty years of personal experience in hyperglycemic crises: diabetic ketoacidosis and hyperglycemic hyperosmolar state, *J. Clin. Endocrinol. Metab.*, 2008, **93**, 1541.
17 A. E. Kitabchi, G. E. Umpierrez, J. M. Miles and J. N. Fisher, Hyperglycemic crises in adult patients with diabetes, *Diabetes Care*, 2009, **32**, 1335.
18 J. Casqueiro, J. Casqueiro and C. Alves, Infections in patients with diabetes mellitus: A review of pathogenesis, *Indian J. Endocrinol. Metab.*, 2012, **16**(1), S27–S36.
19 S. P. Fisher-Hoch, C. E. Mathews and J. B. McCormick, Obesity, diabetes and pneumonia: the menacing interface ofnon-communicable and infectious diseases, *Trop. Med. Int. Health*, 2013, **18**(12), 1510–1519.
20 M. Longo, P. Caruso, M. I. Maiorino, G. Bellastella, D. Giugliano and K. Esposito, Treating type 2 diabetes in COVID-19 patients: the potential benefits of injective therapies, *Cardiovasc. Diabetol.*, 2020, **19**, 115.

21 F. Zhou, T. Yu, R. Du, G. Fan, Y. Liu, Z. Liu, *et al.*, Clinical course and risk factors for mortality of adult inpatients with COVID-19 in Wuhan, China: a retrospective cohort study, *Lancet*, 2020, **395**, 1054–1062.

22 S. Richardson, J. S. Hirsch, M. Narasimhan, J. Crawford, T. McGinn, K. W. Davidson, *et al.*, Presenting characteristics, comorbidities, and outcomes among 5700 patients hospitalized with COVID-19 in the New York City area, *JAMA*, 2020, **323**(20), 2052–2059.

23 A. Remuzzi and G. Remuzzi, COVID-19 and Italy: what next?, *Lancet*, 2020, **395**, 1225–1228.

24 X. Denga, N. Wanga, L. Meng, S. Zhou, J. Huang, J. Xing, L. He, W. Jiang and Q. Li, Optimization of the benzamide fragment targeting the S2′ site leads to potent dipeptidyl peptidase-IV inhibitors, *Bioorg. Chem.*, 2020, **94**, 103366.

25 Z. X. He, Z. W. Zhou, Y. X. Yang, T. X. Yang, S. Y. Pan, J. X. Qiu and S. F. Zhou, A perspective overview of clinically approved oral antidiabetic agents for the treatment of type 2 diabetes mellitus, *Clin. Exp. Pharmacol. Physiol.*, 2015, **42**(2), 125–138.

26 D. J. Drucker, Therapeutic potential of dipeptidyl peptidase IV inhibitors for the treatment of type 2 diabetes, *Expet Opin. Invest. Drugs*, 2003, **12**(1), 87–100.

27 W. S. S. Júnior, M. G. Souza, J. F. N. Neto, E. Bouskela and L. G. Kraemer-Aguiar, Dipeptidyl Peptidase 4 Activity Is Related to Body Composition, Measures of Adiposity, and Insulin Resistance in Subjects with Excessive Adiposity and Different Degrees of Glucose Tolerance, *J. Diabetes Res.*, 2019, DOI: 10.1155/2019/5238013.

28 T. Z. Wu, C. K. Rayner and M. Horowitz, Inter-regulation of gastric emptying and incretin hormone secretion: implications for postprandial glycemic control, *Biomarkers Med.*, 2016, **10**, 1167–1179.

29 J. E. Campbell and D. J. Drucker, Physiology, and Mechanisms of Incretin Hormone Action, *Cell Metab.*, 2013, **17**, 819–837.

30 A. Barnett, DPP-4 inhibitors and their potential role in the management of type 2 diabetes, *Int. J. Clin. Pract., Suppl.*, 2006, **60**(11), 1454–1470.

31 G. L. Plosker. Sitagliptin, a review of its use in patients with type 2 diabetes mellitus, *Drugs*, 2014, **74**(2), 223–242.

32 G. M. Keating, Vildagliptin: a review of its use in type 2 diabetes mellitus, *Drugs*, 2010, **70**(16), 2089–2112.

33 S. Dhillon, Saxagliptin: a review in type 2 diabetes, *Drugs*, 2015, **75**(15), 1783–1796.

34 G. M. Keating, Alogliptin: a review of its use in patients with type 2 diabetes mellitus, *Drugs*, 2015, **75**(7), 777–796.

35 R. Lajara, Use of the dipeptidyl peptidase-4 inhibitor linagliptin in combination therapy for type 2 diabetes, *Expert Opin. Pharmacother.*, 2012, **13**(18), 2663–2671.

36 N. Shinya, A. Mariko and I. Hiroyuki, Anagliptin in the treatment of type 2 diabetes: safety, efficacy, and patient acceptability, *Diabetes, Metab. Syndr. Obes.: Targets Ther.*, 2015, **8**, 163–171.

37 S. H. Kim, S. H. Lee and H. J. Yim, Gemigliptin, a novel dipeptidyl peptidase 4 inhibitor: first new anti-diabetic drug in the history of Korean pharmaceutical industry, *Arch. Pharmacal Res.*, 2013, **36**(10), 1185–1188.

38 L. J. Scott, Teneligliptin: a review in type 2 diabetes, *Clin. Drug Invest.*, 2015, **35**(11), 765–772.

39 P. L. Mccormack, Evogliptin: first global approval, *Drugs*, 2015, **75**(17), 2045–2049.

40 T. Biftu, R. Sinha-Roy, P. Chen, X. Qian, D. Feng, J. T Kuethe, G. Scapin, Y. D. Gao, Y. Yan and D. Krueger, Omarigliptin (MK-3102): a novel long-acting DPP-4 inhibitor for once-weekly treatment of type 2 diabetes, *J. Med. Chem.*, 2014, **57**(8), 3205–3212.

41 K. Kaku, First novel once-weekly DPP-4 inhibitor, trelagliptin, for the treatment of type 2 diabetes mellitus, *Expert Opin. Pharmacother.*, 2015, **16**(16), 2539–2547.

42 R. Sharma, H. Sun, D. W. Piotrowski, T. F. Ryder, S. D. Doran, H. Q. Dai and C. Prakash, Metabolism, excretion, and pharmacokinetics of (3,3-Difluoropyrrolidin-1-yl)((2*S*,4*S*)-4-(4-(pyrimidin-2-yl)piperazin-1-yl)pyrrolidin-2-yl)methanone, a dipeptidyl peptidase inhibitor, in rat, dog and human, *Drug Metab. Dispos.*, 2012, **40**(11), 2143–2161.

43 A. J. Scheen, The safety of gliptins: updated data in 2018, *Expert Opin. Drug Saf.*, 2018, **17**, 387–405.

44 E. Bonora and M. Cigolini, DPP-4 inhibitors and cardiovascular disease in type 2 diabetes mellitus. Expectations, observations and perspectives, *Nutr., Metab. Cardiovasc. Dis.*, 2016, **26**, 273–284.

45 S. Thakral, R. Narang, M. Kumar and V. Singh, Synthesis, molecular docking and molecular dynamic simulation studies of 2 chloro 5[(4 chlorophenyl)sulfamoyl]N(alkyl/aryl)4 nitrobenzamide derivatives as antidiabetic agents, *BMC Chem.*, 2020, **14**, 49.

46 H. Gao, P. Liu, Y. Yang and F. Gao, Sulfonamide-1,3,5-triazine–thiazoles: discovery of a novel class of antidiabetic agents via inhibition of DPP-4, *RSC Adv.*, 2016, **6**, 83438–83447.

47 X. Chen, S. Hussain, S. Parveen, S. Zhang, Y. Yang and C. Zhu, Sulfonyl Group-Containing Compounds in the Design of Potential Drugs for the Treatment of Diabetes and Its Complications, *Curr. Med. Chem.*, 2012, **19**, 21.

48 R. Sharma and S. S. Soman, Design and synthesis of sulfonamide derivatives of pyrrolidine and piperidine as anti-diabetic agents, *Eur. J. Med. Chem.*, 2015, **90**, 342–350.

49 W. H. Sheu, I. Gantz, M. Chen, S. Suryawanshi, A. Mirza, B. J. Goldstein, K. D. Kaufman and S. S. Engel, Safety and efficacy of omarigliptin (MK-3102), a novel once-weekly DPP-4 inhibitor for the treatment of patients with type 2 diabetes, *Diabetes Care*, 2015, **38**, 2106–2114.

50 S. S. El-Karim, M. M. Anwar, Y. M. Syam, M. A. Nael, H. F. Ali and M. A. Motaleb, Rational design and synthesis of new tetralin-sulfonamide derivatives as potent anti-diabetics and DPP-4 inhibitors: 2D & 3D QSAR, in vivo radiolabeling and bio distribution studies, *Bioorg. Chem.*, 2018, **81**, 481–493.

51 M. Tristan-Manzano, A. Guirado, M. Martinez-Esparza, J. Galvez, P. Garcia-Penarrubia and A. J. Ruiz-Alcaraz, Quinoxalines Potential to Target Pathologies, *Curr. Med. Chem.*, 2015, **22**(26), 3075–3108.

52 D. Gupta, N. N. Ghosh and R. Chandra, Synthesis and pharmacological evaluation of substituted 5-[4-[2-(6,7-dimethyl-1,2,3,4-tetrahydro-2-oxo-4-quinoxalinyl)ethoxy] phenyl] methylene thiazolidine-2,4-dione derivatives as potent euglycemic and hypolipidemic agents, *Bioorg. Med. Chem. Lett.*, 2005, **15**, 1019–1022.
53 Y. Yang, S. Zhang, B. Wu, M. Ma, X. Chen, X. Qin, M. He, S. Hussain, C. Jing and B. Ma, An efficient synthesis of quinoxalinone derivatives as potent inhibitors of aldose reductase, *ChemMedChem*, 2012, **7**, 823–835.
54 H. G. Cheon, C. M. Lee, B. T. Kim and K. J. Hwang, Lead discovery of quinoxalinediones as an inhibitor of dipeptidyl peptidase-IV (DPP-IV) by high-throughput screening, *Bioorg. Med. Chem. Lett.*, 2004, **14**, 2661–2664.
55 Y. M. Syam, S. S. El-Karim, T. Nasr, S. A. Elseginy, M. M. Anwar, M. M. Kamel and H. F. Ali, Design, Synthesis and Biological Evaluation of Spiro Cyclohexane-1,2-Quinazoline Derivatives as Potent Dipeptidyl Peptidase IV Inhibitors, *Mini-Rev. Med. Chem.*, 2019, **19**, 250–269.
56 Z. Ali, M. d. J. Akhtar, M. D. R. Haider, A. A. Khan, A. A. Siddiqui and M. S. Yar, Design and synthesis of quinazoline-3,4-(4*H*)-diamine endowed with thiazoline moiety as new class for DPP-4 and DPPH inhibitor, *Bioorg. Chem.*, 2017, **71**, 181–191.
57 D. Xie, Y. Wang, J. Xie, J. Lu, J. Cui, M. Zhang, L. Fu and Y. Wang, Quinoxaline-2,3-diones: potential d-amino acid oxidase (DAAO) inhibitors, *Med. Chem. Res.*, 2014, **23**, 4977.
58 M. V. Dorogov, S. I. Filimonov, D. B. Kobylinsky, S. A. Ivanovsky, P. V. Korikov, M. Y. Soloviev, et al., Convenient synthesis of novel 3-(heterocyclylsulfonyl) propanoic acids and their amide derivatives, *Synthesis*, 2004, **18**, 2999–3004.
59 K. F. Austen and W. E. Brocklehurst, Anaphylaxis in chopped guinea pig lung. I. Effect of peptidase substrates and inhibitors, *J. Exp. Med.*, 1961, **113**, 521–539.
60 X. Deng, J. Shen, H. Zhu, J. Xiao, R. Sun, F. Xie, *et al.*, Surrogating and redirection of pyrazolo[1,5-*a*]pyrimidin-7(4*H*)-one core, a novel class of potent and selective DPP-4 inhibitors, *Bioorg. Med. Chem.*, 2018, **26**, 903–912.
61 A. M. Srour, N. S. Ahmed, S. S. Abd El-Karim, M. M. Anwar and S. M. El-Hallouty, Design, synthesis, biological evaluation, QSAR analysis and molecular modelling of new thiazol-benzimidazoles as EGFR inhibitors, *Bioorg. Med. Chem.*, 2020, **28**, 115657.
62 http://www.rcsb.org.
63 Chemical Computing Group, http://www.chemcomp.com/.
64 S. S. Abd El-Karim, M. M. Anwar, E. Zaki, S. A. Elseginy and Z. M. Nofal, Synthesis and molecular modeling of new benzimidazoles as glutathione S-transferase inhibitors and anticancer agents, *Future Med. Chem.*, 2018, **10**(2), 157–181.
65 N. S. Moorthy, N. F. Bras, M. J. Ramos and P. A. Fernandes, Virtual screening and QSAR study of some pyrrolidine derivatives as α-mannosidase inhibitors for binding feature analysis, *Bioorg. Med. Chem.*, 2012, **20**, 6945–6959.
66 R. D. Cramer, J. D. Bunce, D. E. Patterson and I. E. Frank, Cross validation, bootstrapping, and partial least squares compared with multiple regression in conventional QSAR studies, *Quant. Struct.-Act. Relat.*, 1988, **7**, 18–25.
67 G. Cruciani, P. Crivori, P. A. Carrupt and B. Testa, Molecular fields in quantitative structure-permeation relationships: the Volsurf approach, *J. Mol. Struct.: THEOCHEM*, 2000, **503**, 17–30.
68 C. A. Lipinski, F. Lombardo, B. W. Dominy and P. J. Feeney, Polar molecular surface properties predict the intestinal absorption of drugs in humans, *Adv. Drug Delivery Rev.*, 2001, **46**(1–3), 3–26.
69 K. Palm, P. Stenberg, K. Luthman and P. Artursson, Polar molecular surface properties predict the intestinal absorption of drugs in humans, *Pharm. Res.*, 1997, **14**(5), 568–571.
70 M. Y. Nissan, K. O. Mohammed, W. A. Ahmed, D. M. Ibrahim, M. M. Sharaky, T. M. Sakr, *et al.*, New Benzenesulfonamide Scaffold-Based Cytotoxic Agents: Design, Synthesis, Cell Viability, Apoptotic Activity and Radioactive Tracing Studies, *Bioorg. Chem.*, 2020, **96**, 103577.
71 T. Nasr, S. Bondock, T. M. Ibrahim, W. Fayad, A. B. Ibrahim, N. A. Abdelaziz and T. M. Sakr, New Acrylamide-sulisoxazole Conjugates as Dihydropteroate Synthase Inhibitors, *Bioorg. Med. Chem.*, 2020, **28**(9), 115444.
72 H. G. Abdulwahab, M. F. Harras, N. G. El Menofy, A. M. Hegab, B. M. Essa, A. AbdAllah Selim, et al., Novel Thiobarbiturates as Potent Urease Inhibitors with Potential Antibacterial Activity: Design, Synthesis, Radiolabeling and Biodistribution, *Bioorg. Med. Chem.*, 2020, **28**(23), 115759.
73 T. Nasr, S. Bondock, H. M. Rashed, W. Fayad, M. Youns and T. M. Sakr, Novel Hydrazide-Hydrazone and Amide Substituted Coumarin Derivatives: Synthesis, Cytotoxicity Screening, Microarray, Radiolabelling and In vivo Pharmacokinetic Studies, *Eur. J. Med. Chem.*, 2018, **151**, 723–739.
74 K. O. Mohamed, Y. M. Nissan, A. A. El-Malah, W. A. Ahmed, D. M. Ibrahim, T. M. Sakr and M. A. Motaleb, Design, Synthesis and Biological Evaluation of Some Novel Sulfonamide Derivatives as Apoptotic Agents, *Eur. J. Med. Chem.*, 2017, **135**, 424–433.
75 T. Biftu and R. SinhaRoy, CNS, Pain, Metabolic Syndrome, Cardiovascular, Tissue Fibrosis and Urinary Incontinence, *Compr. Med. Chem.*, 2017, 512–555.
76 W. S. Silva Júnior, M. C. Souza, J. F. Nogueira Neto, E. Bouskela and L. G. Kraemer de Aguiar, Dipeptidyl Peptidase 4 Activity Is Related to Body Composition, Measures of Adiposity, and Insulin Resistance in Subjects with Excessive Adiposity and Different Degrees of Glucose Tolerance, *J. Diabetes Res.*, 2019, **2019**, 1–8.
77 A. T. Natasha, F. Evgenia and E. M. Erin, Dipeptidyl Peptidase-4 at the Interface Between Inflammation and Metabolism, Clinical Medicine Insights, *Endocrinol. Diabetes*, 2020, **13**, 1–10.
78 A. B. Ibrahim, M. Alaraby Salem, T. W. Fasih, A. Brown and T. M. Sakr, Radioiodinated Doxorubicin as a New Tumor Imaging Model: Preparation, Biological Evaluation, Docking and Molecular Dynamics, *J. Radioanal. Nucl. Chem.*, 2018, **317**(3), 1243–1252.

79 T. M. Sakr, M. H. Sanad, W. H. Abd-Alla, D. H. Salama and G. M. Saleh, Radioiodinated Esmolol as a Highly Selective Radiotracer for Myocardial Perfusion Imaging: In Silico Study and Preclinical Evaluation, *Appl. Radiat. Isot.*, 2018, **137**, 41–49.

80 T. M. Sakr, I. T. Ibrahim and W. H. Abd-Alla, Molecular Modeling and Preclinical Evaluation of Radioiodinated Tenoxicam for Inflammatory Disease Diagnosis, *J. Radioanal. Nucl. Chem.*, 2018, **316**(1), 233–246.

81 M. M. Swidan, T. M. Sakr, M. A. Motaleb, A. Abd El-Bary and M. T. El-Kolaly, Radioiodinated Acebutolol as a New Highly Selective Radiotracer for Myocardial Perfusion Imaging, *J. Labelled Compd. Radiopharm.*, 2014, **57**, 593–599.

82 T. M. Sakr, M. A. El-Hashash, A. A. El-Mohty and B. M. Essa, 99mTc-Gallic-gold Nanoparticles as a New Imaging Platform for Tumor Targeting, *Appl. Radiat. Isot.*, 2020, **164**, 109269.

83 B. M. Essa, T. M. Sakr, M. A. Khedr, F. A. El-Essawy and A. A. El Mohty, 99mTc-Amitrole as a Novel Selective Imaging Probe for Solid Tumor: In Silico and Preclinical Pharmacological Study, *Eur. J. Pharm. Sci.*, 2015, **76**, 102–109.